Early-Age Drying and Cracking Properties of Wollastonite-Textile Reinforced Cement Paste Composites

by

Robert Kachala

A Thesis Presented in Partial Fulfillment
of the Requirements for the Degree
Master of Science

Approved July 2014 by the
Graduate Supervisory Committee:

Barzin Mobasher, Chair
Subramaniam Dharmarajan
Narayanan Neithalath

ARIZONA STATE UNIVERSITY

August 2014

ABSTRACT

The main objective of this study is to investigate drying properties and plastic shrinkage cracking resistance of fresh cement-based pastes reinforced with fibers and textiles. Naturally occurring mineral wollastonite has been studied independently as well as in combination with AR-glass textile. A series of blended mixes with Portland cement and wollastonite nano-fibers were developed and tested under low vacuum conditions to simulate severe evaporation conditions and expedite the drying process causing plastic shrinkage cracks. Cumulative moisture loss, evaporation rates, and diffusivity were analyzed by means of a 2-stage diffusion simulation approach, developed previously in Arizona State University. Effect of fiber-matrix interaction on the transport properties of the composite were evaluated using the existing approach. Morphology of the cracked surface was investigated by the means of image analysis wherein length, width, area and density of the cracks were computed to help characterize the contribution of fiber and textile in the cracking phenomenon. Additionally, correlation between cumulative moisture loss and crack propagation was attempted. The testing procedures and associated analytical methods were applied to evaluate effectiveness of four wollastonite fiber sizes and also a hybrid reinforcement system with alkali-resistant glass (ARG) textile in improving shrinkage cracking related parameters. Furthermore, the experimental and analytical approach was extended to magnified version of the existing shrinkage testing set-up to study the size effect of these composites when subjected to matching drying conditions. Different restraining mechanisms were used to study the simulation of the cracking phenomena on a larger specimen. Paste and mortar

formulations were developed to investigate size effect on shrinkage resistance of cementitious composites.

ACKNOWLEDGEMENTS

I would like to express my special appreciation to my advisor Dr. Barzin Mobasher, who has been a great mentor to me. I would like to thank him for providing me with the opportunity to work in a variety of stimulating avenues of research work, as well as continuous encouragement and intellectual insights. I also want to extend my appreciation to Dr. Subramaniam D. Rajan and Dr. Narayanan Neithalath who has served as my committee members by helping and supervising my progress in the Master's degree program.

I would also like to thank Dr. Amir Bonakdar and Vikram Dey, who taught me many skills in preparing and conducting experiments, data analysis and all of their supports and ideas throughout my research work. I would like to acknowledge outstanding work done by my peer, Dr. Mehdi Bakshi, for establishing the basis and a straight forward path that I could follow up and extended my work to further areas.

I greatly appreciate the assistance provided by Mr. Peter Goguen and Mr. Kenny Witczak for all of their great works in the laboratory, especially with the trouble-shooting as well as the maintenance on testing devices. Without their help, I could definitely not finish my experiments.

I would like to express my gratitude to my dear colleagues and friends, Yiming Yao, Karan Aswani and Xinmeng Wang for their help and more importantly, the great time we spent together.

I would also like to acknowledge NYCO Minel Inc. for providing financial support and material necessary to complete this study.

TABLE OF CONTENTS

Page

CHAPTER Page

CHAPTER Page

LIST OF FIGURES

Figure Page

Figure Page

LIST OF TABLES

Table Page

1. INTRODUCTION

1.1 Motivation

Construction is a part of global econonomy and one of the largest industries in any country of the world. It has a significant influence on population growth, social and economic development. Construction provides many employment opportunities and contributing to almost five percent of the gross domestic product of United States through sectors such as construction materials, building systems and service. Tremendous growth in construction has given rise to one of the major challenges of the 21st century [1]. There is an urgent need to provide support for further development, but with techniques that can address global warming issues, resource cost and energy efficiency usage. Of late civil engineering, as a part of global construction community, has concentrated on sustainability to promote the exponential growth of infrastructure [2]. Through a lot of research, civil engineering has been attempting to optimize the usage of limited natural resources that make up building materials to satisfy the ever increasing demand. Special attention has been given to cement concrete – one of the most material used on the planet - due to its well-known CO_2 creation through calcination of limestone and clinker production [3]. This issue of controlling CO_2 emissions can be addressed by developing durable building systems with low cement content, designing light weight structural members and utilizing renewable energy resources. Therefore, an improvement to environmental, social and economic performances is made through sustainable construction materials which lead to structures that match the needs of the present without compromising the demands of the future. This study is based on the performance evaluation of fiber and textile reinforcement in brittle cementitious matrices through the

use of novel characterization and simulation techniques to develop materials that can be applied in various infrastructure applications. The achievement of such task can be done through understanding of traditional degradation mechanisms present in cementitious systems. The focus of this study is investigation of long-term durability concerns of cement-based materials by controlling early-age shrinkage cracking, caused by drying of fresh concrete.

1.2 Problem Definition

Large surface areas of freshly-placed concrete such as slabs on grade, thin surface repairs or patching that are exposed to abnormal drying conditions are often susceptible to early plastic shrinkage cracks. Repercussions of plastic shrinkage cracks include reduction in long-term load carrying capacity, accelerated deterioration through penetration of aggressive agents such as chloride ions and freeze-thaw cycles. Such conditions directly cause an increase of maintenance costs, reduced service life and longtime durability concerns [4,5,6]. Several factors such as differential settlement, thermal dilation, and autogenous deformation [7] can be attributed to the formation of plastic shrinkage cracks, but primarily the process is initiated by a high rate of water evaporation from the concrete surface [8,9,10]. Although factors such as air, concrete temperature, wind speed, and relative humidity [10] affect evaporation, in the presence of restrains, the three dimensional nature [11] of shrinkage leads to tensile stresses that exceed the low tensile strength of fresh concrete and causes formation of cracks.

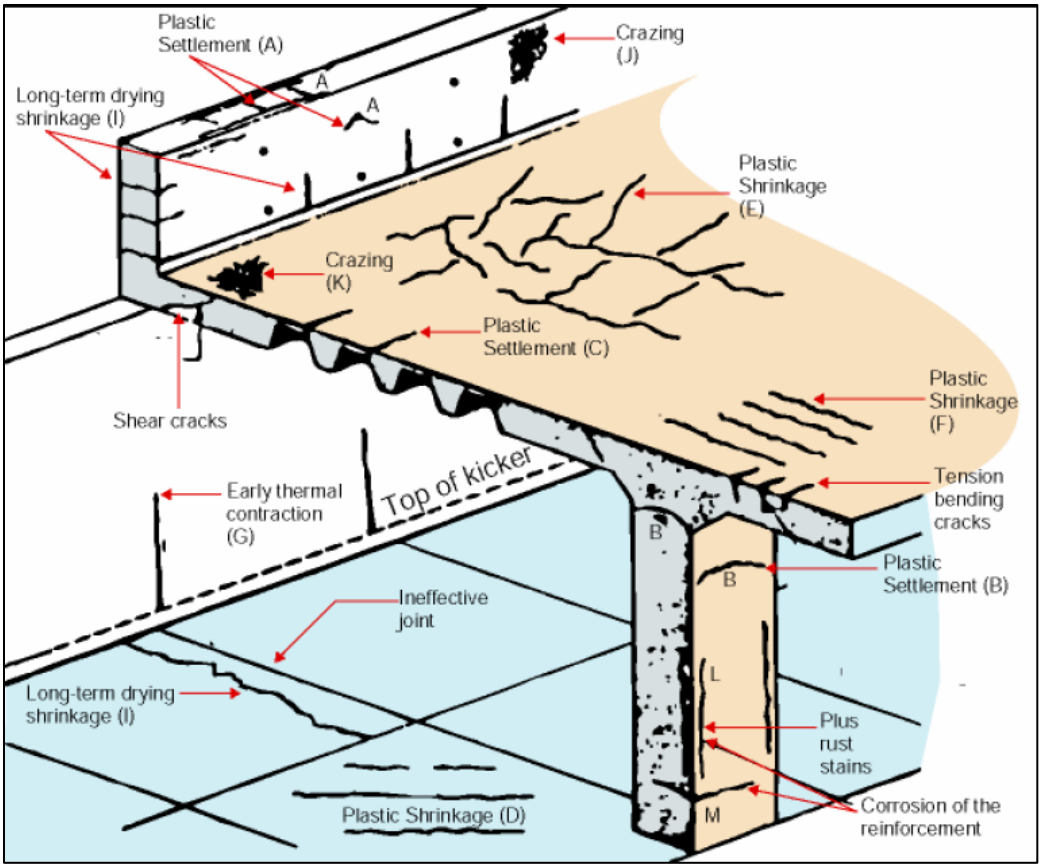

Figure 1.1 – Locations of Plastic Shrinkage Cracks in a Typical Structure [11]

1.3 Mechanism of Early-Age Shrinkage Cracking

High rate of evaporation and loss of water at the surface of fresh concrete creates adhesive forces and surface tension in the form of water menisci in the inner-spaces of solid particles [12]. Inherent curvature of water particles causes built up of negative pressure is in the capillary water, which causes water particles to continue to rise and further evaporate [13,14]. Within a few hours, capillary pressure developed in fresh drying concrete, can reach 50 kPa and exceed 1 MPa [9,12,15,16,17]. Capillary pressure further acts on the solid particles and induces strain level in the range 1 to $4x10^{-3}$ [12,14,18,19] in concrete, while it is still in plastic state. In the presence of restrains,

developed pressure may exceed low tensile strength causing formation of sequential cracks.

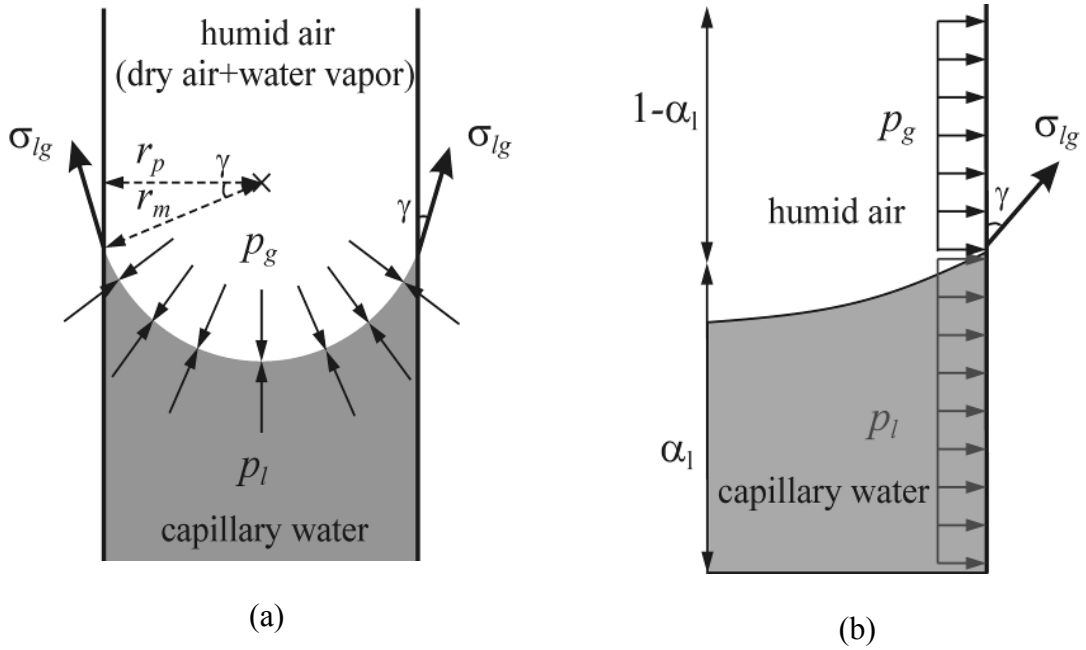

Figure 1.2 - Equilibrium Between Liquid Water and Humid Air Inside a Pore at Different Pressures: a) initial capillary, b) built-up capillary [20]

1.4 Controlling Early-Age Cracking

Although effective prevention techniques rely mostly on prevention of water loss by methods such as aggregates moistening, windbreakers, sunshade, covers and fogs, controlling plastic shrinkage cracks can be done effectively by fiber reinforcement [21,22,23]. Use of short distributed wood pulp [24], synthetic [25] and cellulose [24] fibers has been successfully used in reducing shrinkage cracking. Such studies support the hypothesis that short fibers are an effective form of reinforcement against potential plastic shrinkage cracking due to their ability to decrease the crack length and width [22,24,26]. In the current study, wollastonite nano-fibers and hybrid wollastonite-textile

reinforcement schemes are explored as a potential alternative of reinforcement against plastic shrinkage.

1.5 Plastic Shrinkage Testing Background

A majority of recent publications have focused on one-dimensional cracking of the concrete by utilizing special restraints [7,8,9] implementing fans [27, 28], fans and heaters [25, 29], heat lamps [30] , wind tunnel [31] and vacuum drying [32] to simulate severe evaporation conditions and expedite the drying process causing plastic shrinkage cracks. The design of such tests does not provide any quantitative information about the principal driving force of plastic shrinkage, lacks accurate measurement of moisture evaporation data and characterization of the ability of fibers/textile to distribute micro-cracks throughout the base matrix. In this context, a low-pressure two-dimensional drying technique developed at Arizona State University stands out and can help in the characterization of contribution of fibers in the cracking phenomenon and evaporation as a material characteristic [33,34]. Rapid rate of evaporation is simulated in the current study to evaluate the performance of wollastonite nano-fibers individually and in combination of textile as reinforcement in freshly made cement pastes. Moisture loss was analyzed by means of a 2-stage diffusion simulation process [33,34] to investigate fiber-matrix interaction and the effect of transport properties based upon the cumulative moisture loss, evaporation rates, and diffusivity. Morphology of the cracked surface was investigated by means of image analysis wherein length, width, area and density of the cracks were computed. Additionally, correlation between moisture loss and crack morphology was attempted.

1.6 Thesis Objectives

There are several different objectives that were achieved though out this researched and they are as the following. Chapter 1 uses analytical techniques and image analysis to investigate and evaluate drying properties and plastic shrinkage cracking resistance of fresh fiber reinforcement cement-based paste composite. Control mix which includes cement paste only is compared with composite that consists of partial cement replacement with nano-size fibers. Chapter 2 uses techniques presented in Chapter 1 to investigate and evaluate drying properties and plastic shrinkage cracking resistance of fresh textile-fiber reinforcement cement-based paste composite. Control mix is again compared to a composite, but in addition to cement replacement with fiber, a layer of textile is added; proper comparison is made between the two composites. Chapter 3 addresses the limited nature of specimen size used in Chapter 1 and Chapter 2 by developing a scaled-up version of the current set-up. Difficulties of the development are presented and discussed.

2. WOLLASTONITE REINFORCED CEMENTITIOUS COMPOSITE

2.1 Introduction

Acicular shaped wollastonite nano-particles are made from naturally occurring calcium meta-silicate ($CaSiO_3$) mineral [35]. With high modulus of elasticity in the range of 303-530 GPa, tensile strength in the range of 2700-4100 MPa [36] and aspect ratio in the range of 3:1 to 20:1, wollastonite fiber has already found its applications in ceramic products, paints, pottery and dental care [35, 37]. However, due to its nominal length of 33-2000 μm, which is about the same range as cement particles (about 25-40 μm) [38], wollastonite nano-fiber can not only be considered as a potential alternative to short fibers but also as a cement replacement. With temperature and chemically resistant composition that consists mostly (up to 90%) of calcium oxide (CaO) and silicon dioxide (SiO_2) [39] in addition to the size and aspect ratio, wollastonite fiber has characteristics that makes it suitable for use in cementitious materials, with little additional processing.

2.2 Testing Methodology

A test method for characterizing evaporation parameters and simulating the sequential formation of shrinkage cracks in two-dimensional cement paste samples under low-pressure condition has been developed earlier [33,34]. Schematics of the setup are shown in Figure 2.1 and Figure 2.2, where a vacuum chamber is used to impose drying conditions on the surface of a fresh paste. A square specimen with all sides sealed except the face section is filled with fresh paste. The mold consists of interlocking pieces made of polycarbonate. The mold uses anchor hooks to fully connect the fresh paste with the mold, providing shrinkage restraint in two directions. The sample is placed on a load cell which serves as a digital scale, and the entire assembly is placed inside a glass desiccator.

The weight of the sample is continuously monitored throughout the drying cycle. Using a vacuum pump and a pressure regulator, the air pressure inside the desiccator is lowered to absolute 1700 Pa (0.5 inHg) and maintained at this pressure throughout the test. A condensing system including a D-Drying apparatus is used similar to Copeland and Hayes [40], and is capable of removing water vapor from the desiccator at very high rate in a non-steady state condition. The weight of the specimen inside the drying chamber was recorded using a computer interface unit. A digital camera mounted above the specimen is used to take pictures of the sample at 15 min intervals. Such a process simulates the real effects of cracking during the curing of the cast in-situ concrete. Typical time lapse images of a representative specimen subjected to the aforementioned testing procedure are shown in the Figure 2.3.

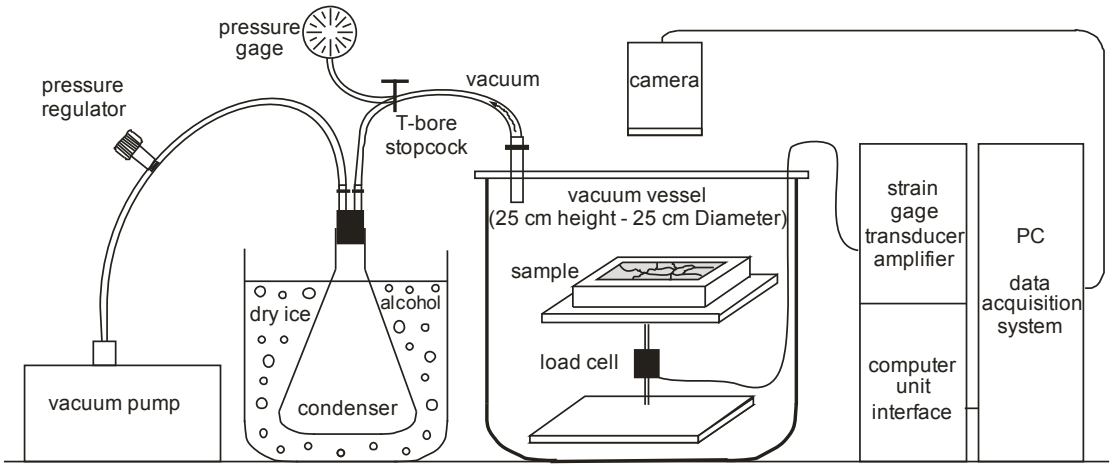

Figure 2.1 - Schematic of Vacuum Drying Test Setup [33]

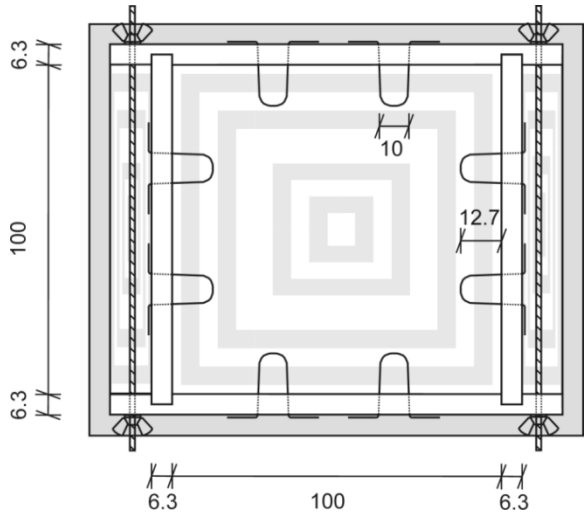

Figure 2.2 - Plan View of the Mold (numbers in mm) [33]

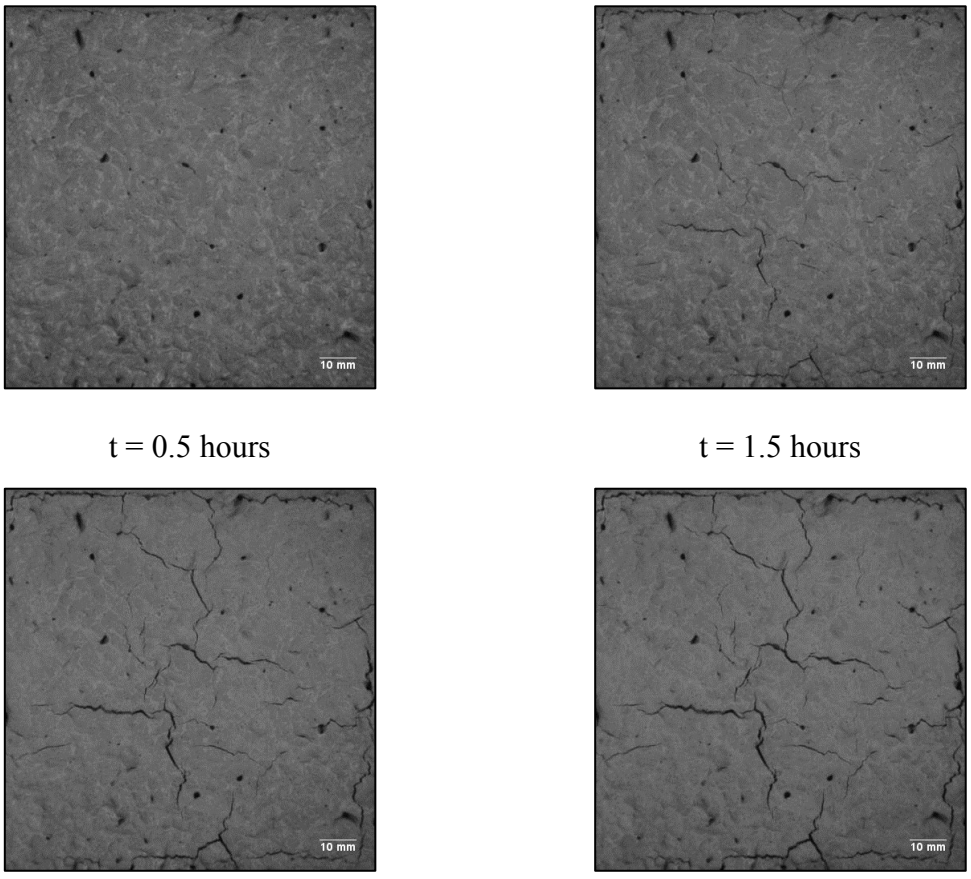

t = 0.5 hours t = 1.5 hours

t = 2 hours t = 3 hours

Figure 2.3 – Sequential Growth of Shrinkage Cracks Observed in a Control Paste Specimen with w/c=0.45

2.3 Analysis Procedures

2.3.1 Cumulative Moisture Loss and Evaporation Rate

The weight loss data recorded throughout the test was subjected to smoothening, data reduction, and curve fitting to produce cumulative moisture loss response. Moisture loss under vacuum conditions was monitored for a period of 24 hours. Numerical differentiation of the fitted cumulative moisture loss is used to calculate the evaporation rate. Evaporation rate can be expressed in terms of exposed surface area of the specimen as shown in Equation (1).

$$J = \frac{\Delta M}{A \Delta t} = \frac{1}{A} \frac{dM}{dt} \tag{1}$$

where J is the evaporation rate (kg/m^{2}s), dM is the mass change at specified time steps (kg), dt is the time step (s) and A is the surface area of the original sample (m^2). Figure 2.4 shows a typical response of cumulative moisture loss and time history of evaporation.

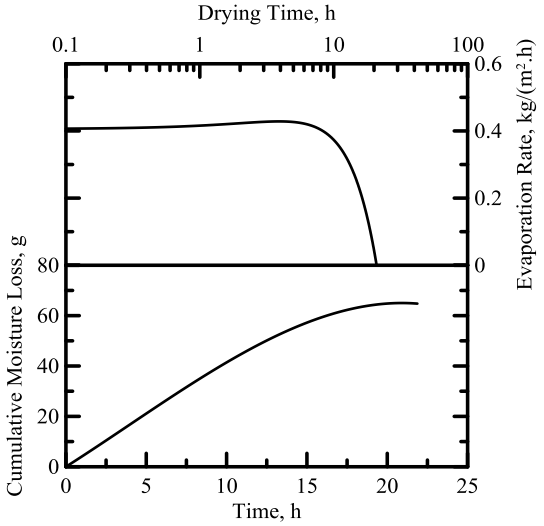

Figure 2.4 - Typical Cumulative Moisture Loss and Evaporation Rate of a Cement Paste Sample

2.3.2 Moisture Diffusivity Calculation

In recent publications [31,32,33,34], it has been shown that the diffusion process of cement pastes can be presented by a dual-stage drying model and corresponding moisture diffusivity can be used to predict the cumulative moisture loss of cement-based materials subjected to vacuum drying conditions. The model can be described as a boundary value problem with the following boundary conditions. Constant flux at the surface, directly obtained from the experimental data, can be applied as the boundary condition of the first stage. Constant concentration at the surface can be applied as the boundary condition for the second stage. Zero flux is imposed as the other boundary condition for both of the stages at the bottom of the specimen. The summary of the boundary conditions is given as the following:

$$\text{Stage I drying:} \quad \text{at } x = L, \quad J = F_0$$
$$\text{Stage II drying:} \quad \text{at } x = L, \quad C_s = C_* = C_{w,low\ pressure}$$

Assuming a constant diffusivity [41], the analytical solution for the initial and boundary conditions of Stage I drying is as the following:

$$C(t,x) = C_i + \frac{F_0 L}{D_I}\left\{\frac{D_I t}{L^2} + \frac{3x^2 - L^2}{6L^2} - \frac{2}{\pi^2}\sum_{n=1}^{\infty}\frac{(-1)^n}{n^2}\exp\left(\frac{-D_I n^2 \pi^2 t}{L^2}\right)\cos\frac{n\pi x}{L}\right\} \quad (1)$$

where D_I is the diffusivity in Stage I drying. Providing constant F_0 and D_I values, moisture concentration at the top surface can be calculated. Assuming constant concentration at the surface [41] the analytical solution for the boundary conditions of Stage II is as the following:

$$\frac{C - C_i}{C_* - C_i} = 1 - \frac{4}{\pi}\sum_{n=0}^{\infty}\frac{(-1)^n}{2n+1}\exp\{-D_{II}(2n+1)^2\pi^2 t / 4l^2\}\cos\frac{(2n+1)\pi x}{2L} \quad (2)$$

where D_{II} is the average diffusivity over space and time [33]. By integrating both solutions over the thickness of sample, a total amount of diffusing moisture in Stage I and II drying, which has left the sample at time t, M_t (kg), can be obtained. Therefore, by calculating the diffusivity values from Stage I and II, the total amount of moisture loss can be predicted at any time. Figure 2.5 shows the comparison between experimental and simulated data for a drying cement paste sample. It should be noted that better simulations fits are available, but they involve non constant diffusivities. Constant stage diffusivity method is used as to compare the specimens based upon the average diffusivity values over the duration of the test.

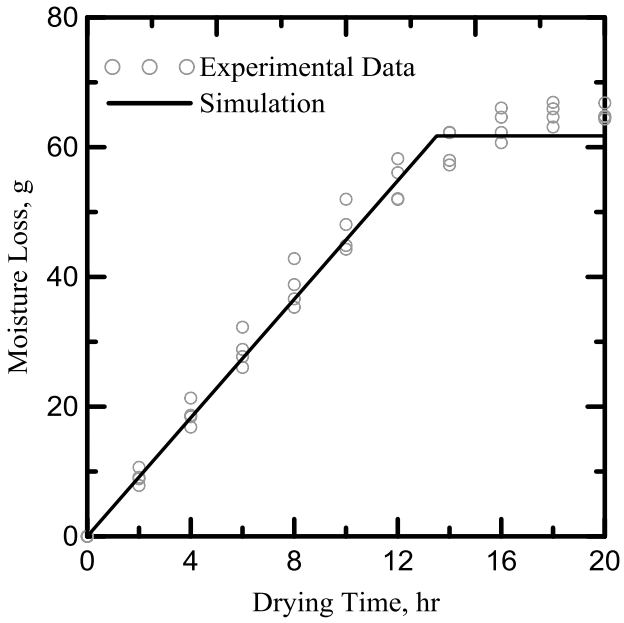

Figure 2.5 - Simulation of Cumulative Moisture Loss vs. Experimental Data for Cement Paste Specimens

2.3.3 Imagine Analysis on Crack Morphology

Two-dimensional crack morphology parameters were quantified and compared for each type of wollastonite replacement with respect to the control base mix. After the

completion of the test, the specimen was scanned using a high resolution (1200 dpi) scanner. High resolution images are enabled to produce a more desired accuracy of the surface texture of the test specimen for the morphology calculations. The scanned image of the specimen is initially subjected to several filtering and clean up steps, wherein the unwanted features are removed using an image analysis software, Image J©. The image is cropped to a region of interest where all of the shrinkage cracks are visible and then converted to binary image. The conversion from RBG image (red, blue and green model) to binary image (white and black model) introduces imperfections into the image – extra objects that will be accounted for within the analysis if not removed. Therefore, manual removal of these objects is necessary. The binary image is next inverted to identify the skeleton of the image. Skeletonization allows for the detection of the intersections points by using a kernel of 1 and the convolution function. Sortclasses function, developed by LA1- Medical Image Processing 2003 [42], is employed to reduce the islands of the intersection points down to 1 pixel. This function uses specified distance of neighboring pixels to check for non-repetitiveness. The detected intersection are dilated and filtered with the original image. Such image is labeled as final image and is used for all of the calculations purposes. In Figure 2.6, it shows the described procedure. Area is calculated as the summation of the pixels within the region of interest; length is measured as length of the major axis of an ellipse that has the same normalized second central moment as the region of interest. Based on the physical dimensions of the specimen and the size of the image (in pixels) calibration factors are determined; the calculated values are converted to physical dimensions.

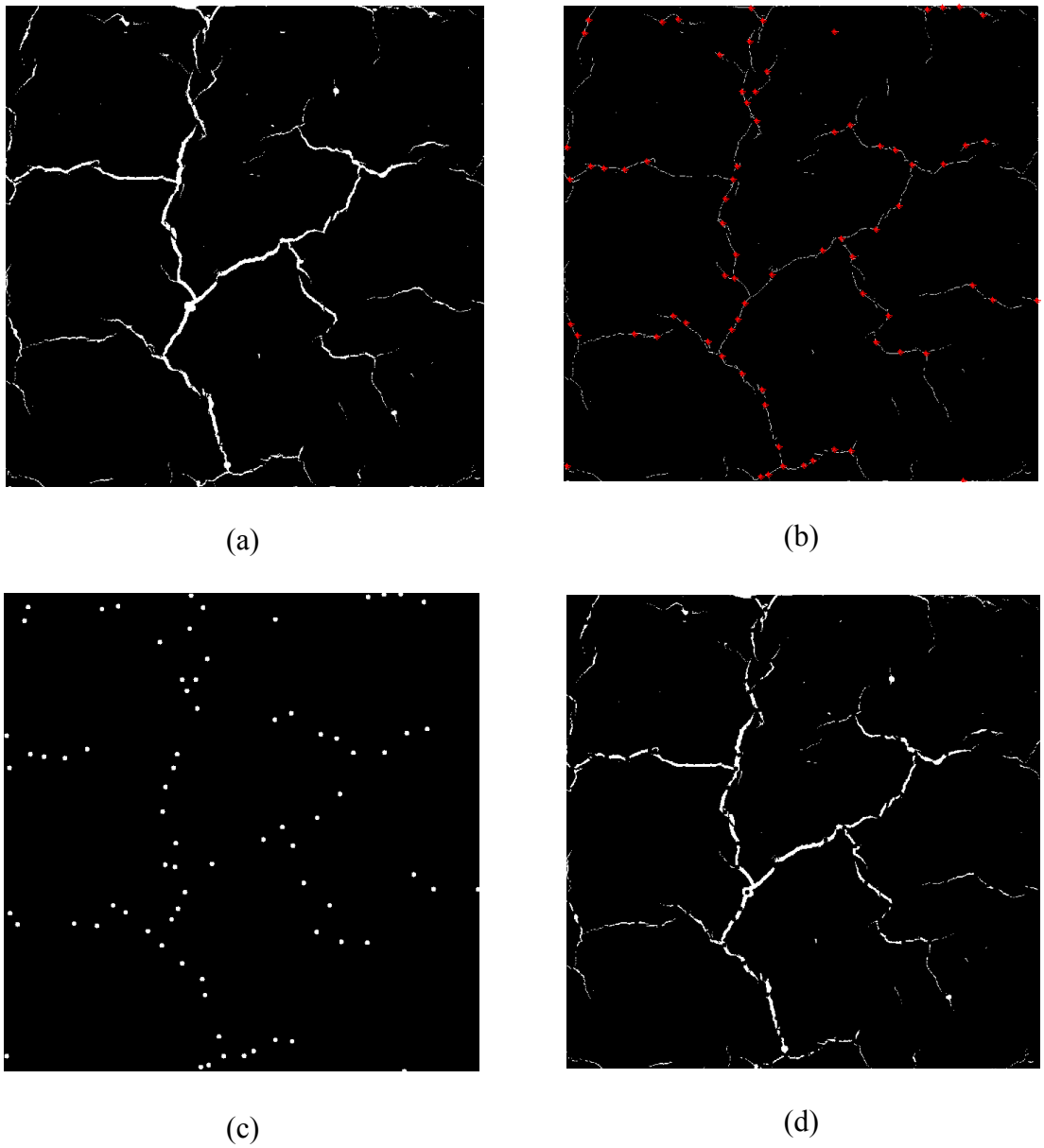

Figure 2.6 – Image Analysis Methodology: a) binary image of crack pattern, b) detection of intersection points of cracks from skeletonized image of crack, c) dilation of the intersection points, d) subtraction of dilated intersection points from the initial binary image

2.4 Experimental Program

The experimental program consisted of evaluating four different types of wollastonite fibers, two coarse sizes of HARRP and two fine sizes of NYAD-G. The

corresponding sizes of the fibers are 2000 µm, 850 µm, 55 µm and 33 µm and will be referred to as C2000, C850, F 55, F33, respectively. Micrographs of wollastonite fibers used in this study are shown in Figure 2.7.

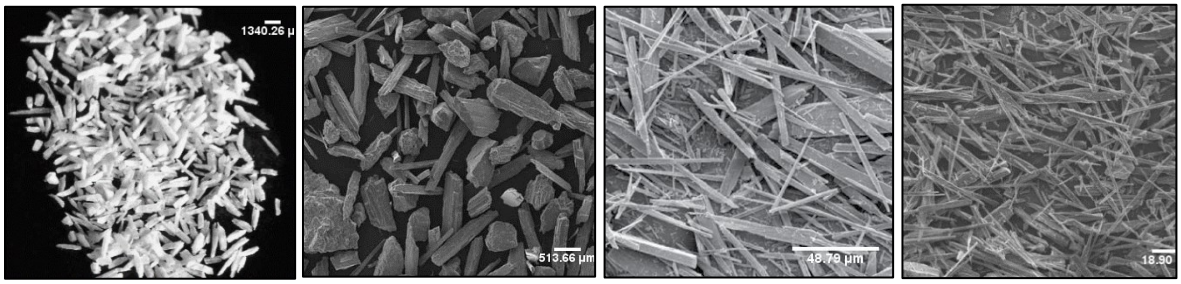

(a) C2000 (b) C850 (c) F55 (d) F33

Figure 2.7 – Microstructure of Wollastonite Fibers Used (Magnification: (a, b) x25; (c, d) x100) [36,39]

The mixture proportions are provided in Table 2.1. The primary binding agent includes Portland cement (Type II/V) with water/powder ratio of 0.45. A water-reducing admixture (superplasticizer), Metflux© 4930F manufactured by BASF Construction Chemicals, was used with some of the mixes to compensate the loss in workability due to addition of wollastonite fibers. The cement content was adjusted for a partial replacement with wollastonite in these mixtures. Maximum recommended replacement was determined to be 15%, as suggested by literature [37,38,43, 44]. The mixing procedure consisted of mixing the dry ingredients, followed by the addition of water and additional mixing at higher speed, until desired consistency is achieved. Fresh cementitious paste is then immediately poured in the molds for the vacuum evaporation test. Minimum of three replicates was used for each type of fiber.

Table 2.1 - Mix Design for Wollastonite Shrinkage Tests

Cement replacement Constituents	Control		Wollastonite	
	Proportions by weight percentage	Proportions by 1000 g of Cement	Proportions by weight percentage	Proportions by 1000 g of Cement
Portland Cement	100	1000	85	850
Wollastonite	0	0	15	150
Water	45	450	45	450
Super Plasticizer	0.05	0.67		

2.5 Results and Discussion

Reproducibility of the test data is shown in Figure 2.8 wherein a typical set of cumulative time history of moisture loss and evaporation response obtained from the experiments performed for 24 hours is presented.

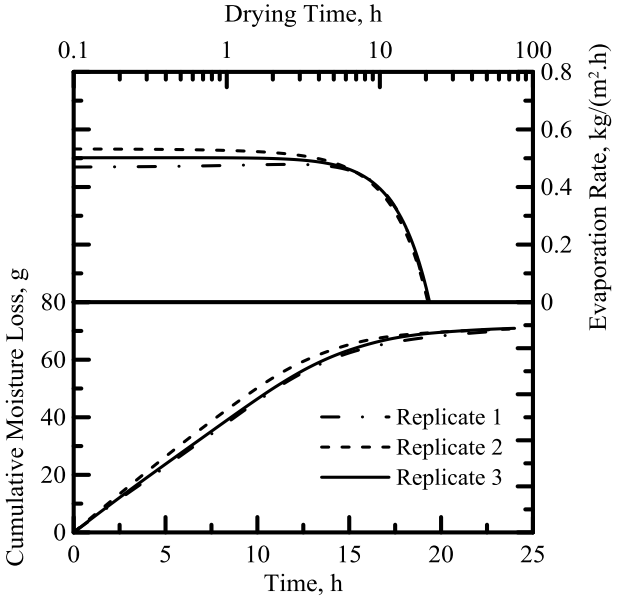

Figure 2.8 – Cumulative Moisture Loss Curve of C2000 Replicates at 15% Dosage

For discussion purposes, presented figure is limited to one type of wollastonite, namely C2000 at 15 % replacement. Table 2.2 shows average values obtained from the

analysis, wherein initial evaporation rate, total moisture loss diffusivity for stage I and stage II are all fairly consistent, as the standard deviation is within 10%. Reproducibility of the morphology cracking data is shown in Figure 2.9, wherein a typical set of cleaned binary version of scanned specimen images is presented. Similar to the evaporation analysis, values such as crack length, width and area obtained from the morphology analysis, are within acceptable error tolerance.

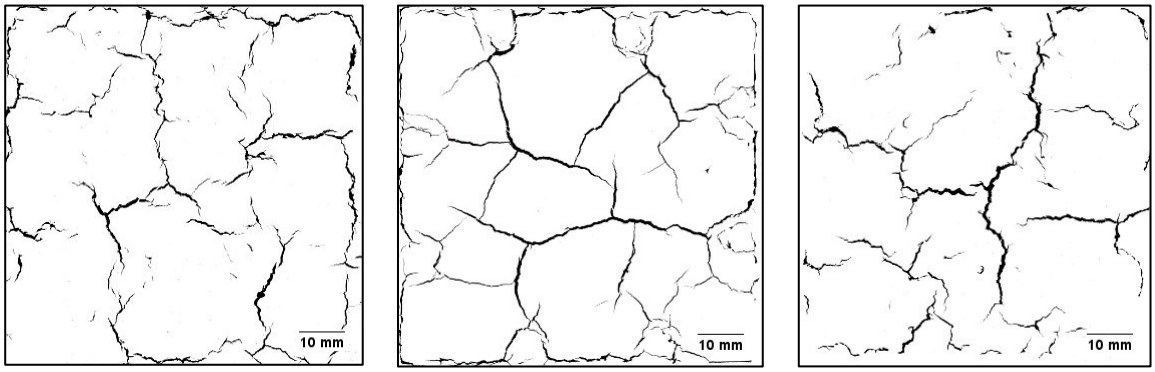

(a) (b) (c)

Figure 2.9 – Morphology of Cracked Surface of C2000 Replicates at 15% dosage

2.5.1 Evaporation

The effect of wollastonite nano fibers in restraining the growth of early age shrinkage cracks of cement-based paste specimens was studied using the evaporation response as presented in Figure 2.10. Specimens are compared on the basis of fiber type. The behavior of the specimens is quite similar with respect to both moisture loss and evaporation rates. Parameters that characterize the evaporation rates, transition time between Stage I and Stage II, diffusivity of Stage I and Stage II and cumulative moisture loss, as well as the accuracy of the fitting model are reported. Table 2.2 summarizes the

aspects of the evaporation analysis and individual variations are discussed in the following sections.

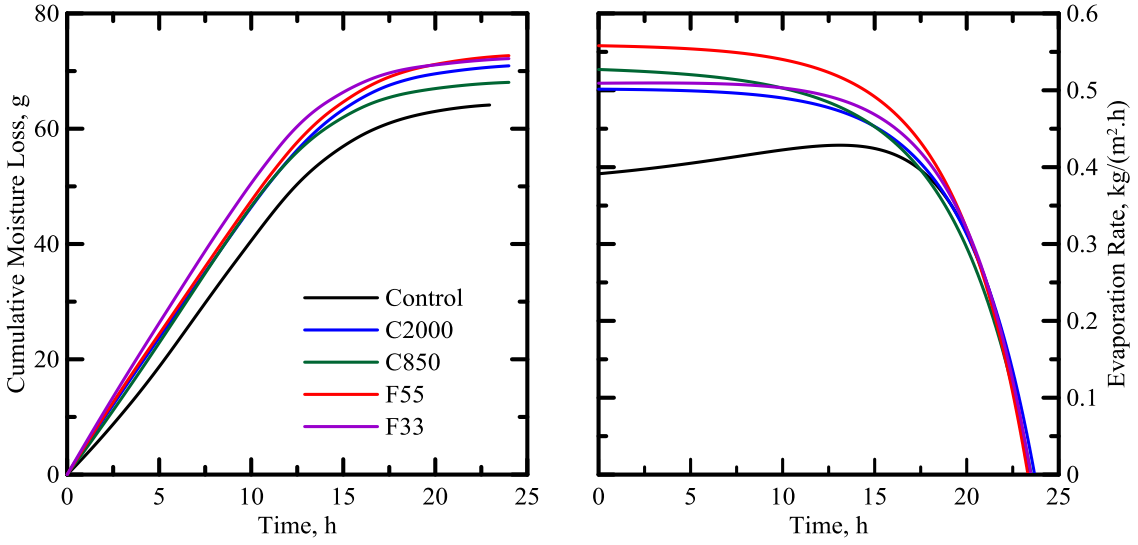

(a) (b)

Figure 2.10 – Effect of Wollastonite Addition on Evaporation Tests Results: a) cumulative moisture loss, b) evaporation rate

Table 2.2 – Drying Parameters Summary of Wollastonite Specimens

Specimen Type	**Initial Evap. Rate (kg/(m²h))**	**Cumulative Moisture Loss at 24 h (g)**	**Transition Time (h)**	**Diffusivity Stage I (m²/hr)**	**Diffusivity Stage II (m²/hr)**	**Prediction Accuracy (%)**
Control	0.404 ± 0.078	65 ± 1	11 ± 2	1.85E-3	2.47E-4 ± 3.70E-4	96 ± 3
C2000	0.492 ± 0.104	68 ± 3	9 ± 1	1.85E-3	2.62E-4 ± 1.30E-5	97 ± 2
C850	0.553 ± 0.075	70 ± 3	8 ± 1	1.85E-3	2.75E-4 ± 1.30E-5	98 ± 1
F55	0.562 ± 0.069	71 ± 2	8 ± 1	1.85E-3	2.82E-4 ± 2.70E-5	97 ± 2
F33	0.535 ± 0.050	69 ± 2	8 ± 0	1.85E-3	2.70E-4 ± 1.40E-5	98 ± 2

Effect of w/c ratio

The estimated cumulative moisture loss for Control, C2000, C850, F55 and F33 specimens were found to be 0.188, 0.232, 0.239, 0.242 and 0.235 g/g normalized w.r.t to the initial weight of paste specimen at the start of the test, respectively. It is known that cementitious specimens with higher w/c ratios yield higher cumulative moisture loss [33]. Cement replacement by wollastonite allowed for slightly higher w/c ratio as compared to control samples resulting in a 29 % increase in the cumulative moisture loss. Higher cumulative moisture loss can be also measured through the Stage I and Stage II diffusivities reported. Stage I diffusivities were quite similar for all specimens; they are closely related to the diffusivity rate for cement paste at vacuum pressure. However, an increase in diffusivity up to 14 % for specimens reinforced with wollastonite fibers is observed during Stage II. The combined effect of increased initial evaporation rates for wollastonite specimens and the variability in diffusivity at different stages contributes to an increase in the cumulative moisture loss when compared to the control mix.

Effect of fiber type

Significant effect of cement replacement with wollastonite nano-fibers can be observed in the Stage I to Stage II transition time. Replacement of cement with wollastonite fibers resulted in a gradual transition between the modes of drying. Such mechanism could be attributed to the effect of fibers in controlling early-age cracks. Replacement cement with wollastonite decreased the transition time from 11 hours to 8 hours, which means that the initial evaporation rates is higher and can be attributed to higher number of micro-cracks. Comparison of the initial evaporation rate and diffusivities based upon the type of wollastonite replacement indicates an interesting

trend. According to Figure 2.11 (a), diffusivity of Stage I remains the same for all of the specimens, but average diffusivity of Stage II was found to increase by 6 %, 11 %, 14 % and 9 % for C2000, C850, F55 and F33, respectively when compared to the control specimens. The accuracy of the prediction is presented in Table 2.2.

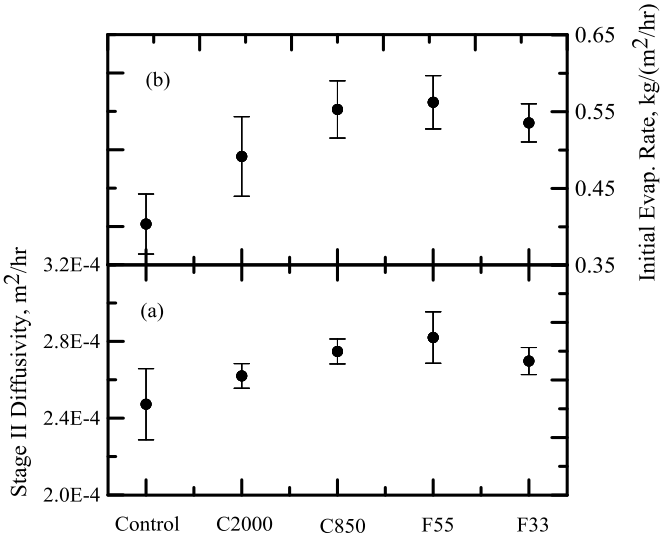

Figure 2.11 – Effect of Wollastonite Addition on Stage II Diffusivities and Initial Evaporation Rate

Similar to diffusivities, initial evaporation rate is also affected by the size of wollastonite fibers. Smaller sized wollastonite fibers produce a higher evaporation rate, of up to 40%, when compared to the control specimen as shown in Figure 2.11 (b). The mechanism controlling the evaporation could be contributed from both higher w/c ratio and also size of the wollastonite inclusions. Since during the Stage II, diffusivity occurs under internal mass transfer control, the microstructure plays a significant role in the drying process. Specimens reinforced with wollastonite exhibit a higher diffusivity as the microstructure allows for the moisture to travel easily through the cracked area. The ability of smaller size wollastonite to have higher Stage II diffusivity can be accredited to a uniform distribution of particles within the paste that limits the cracks on the macro-

scale. However, such mechanism produces more micro-cracks and therefore provides more cracked area, on the micro level, which causes higher diffusivity, evaporation rate and moisture loss.

2.5.2 Crack Morphology

Figure 2.12 (a-e) provides the scanned images of the representative specimens from the crack morphology study. It is evident that the wollastonite fibers are very effective in restraining the growth of shrinkage cracks on the surface of the paste specimens when compared to the control. The reduction of plastic shrinkage cracks of nano-scale fibers can be accredited to its smaller size and the ability of blending better with the paste matrix. This aids in uniform dispersion of the nano-fibers across the cementitious matrix. The F55 and F33 wollastonite fibers are more effective in bridging the cracks at the nano-level, thus, effectively reducing the amount and the size of cracks at the macro level when external loads are applied. Analyzed crack morphology results have been summarized in Table 2.3. Total area of cracks, crack length and width has been considered to compare different groups of specimen. Figure 2.13 summarizes the effect of different wollastonite fiber types in controlling the growth of shrinkage cracks evaluated in the current study. As evident, there is a substantial reduction in all shrinkage cracking related parameters for all specimens reinforced with wollastonite, when compared to plain control paste specimens.

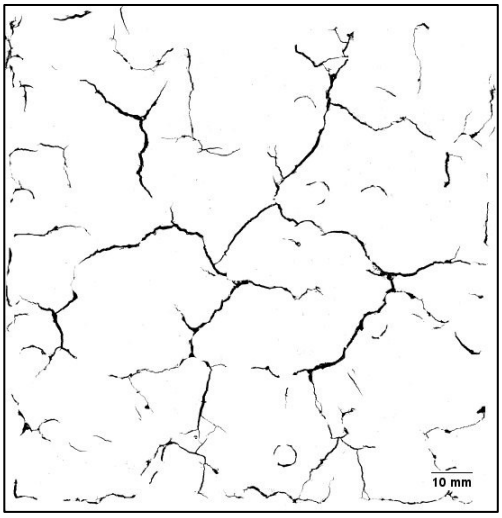

(a) Control Paste

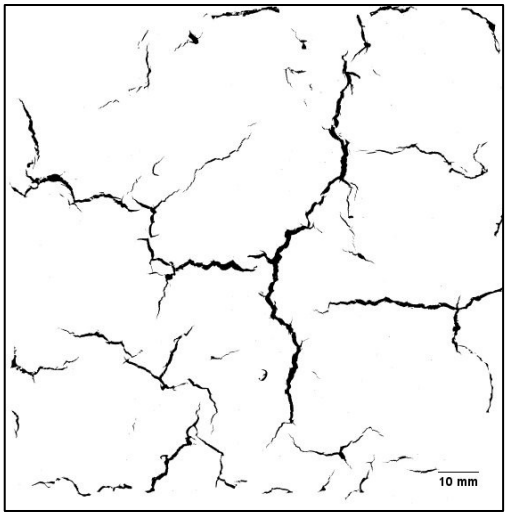

(b) C2000 Paste

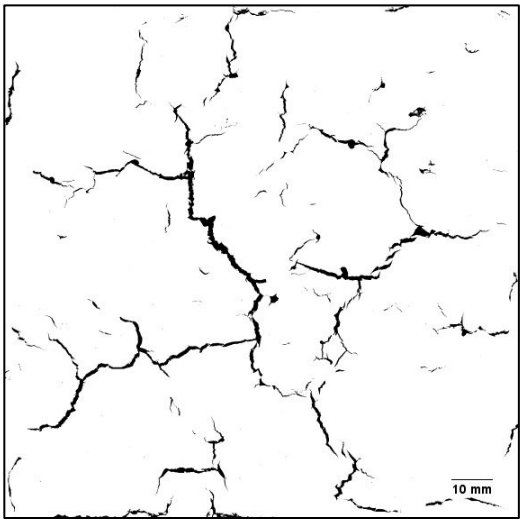

(c) C850 Paste

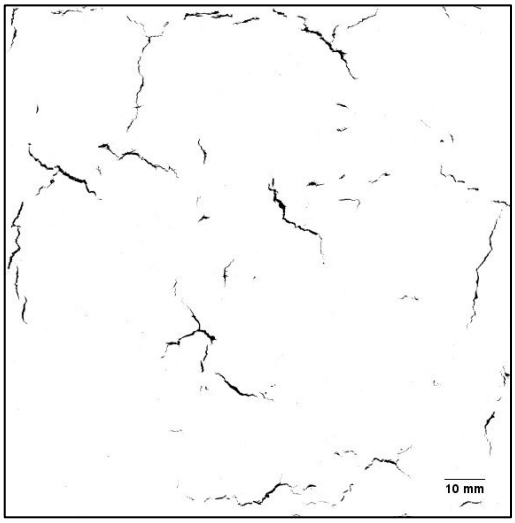

(d) F55 Paste

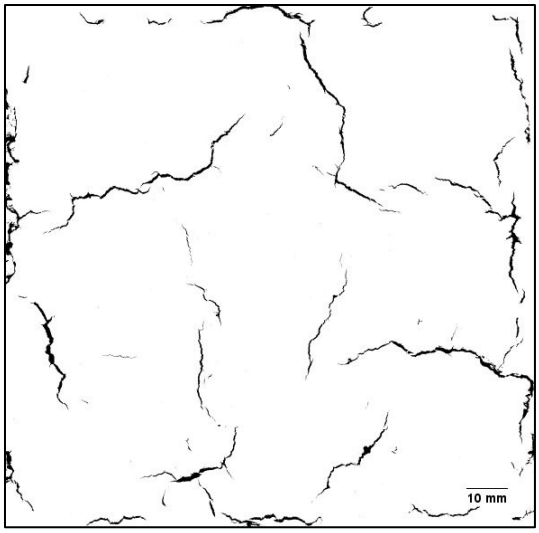

(e) F33 Paste

Figure 2.12 (a)-(e) - Cleaned Up Binary Images of Representative Wollastonite Specimens

It is noted that efficiency of wollastonite fibers can be related to the relative reduction in the magnitude of cracking parameters. Among all four grades of wollastonite, F55 is most effective in improving resistance to early age shrinkage cracks. Total length of cracks and crack width is reduced by a factor of two, and cracked area is reduced by as much a factor of three for specimens reinforced with F55 when compared to control paste specimens. It is evident that the remaining forms of wollastonite fibers are also effective in limiting the growth of shrinkage cracks, albeit not as effective as F55 fibers. For instance, C2000 fibers can reduce the total crack length to as much as 35 %, cracked area by 30 %. C850 fibers can reduce the length of cracks by 40 % and cracked area by about 9 %, and similar to C2000 fibers they do not contribute to the width of cracks. F33 fibers can reduce the length of the cracks by 30 % and width of the cracks by 17 %. Also the cracked area can be reduced by 41 % with F33 fibers.

Table 2.3 – Crack Morphology Parameters Summary of Wollastonite Specimens

Crack Properties	Control	C2000	C850	F55	F33
Length of cracks (mm)	955 ± 45	624 ± 99	576 ± 237	493 ± 90	681 ± 66
Area of cracks (mm^2)	303 ± 35	215 ± 76	276 ± 131	94 ± 26	178 ± 23
Density of cracks (mm^{-1})	0.096 ± 0.004	0.062 ± 0.010	0.058 ± 0.024	0.049 ± 0.009	0.068 ± 0.007
Mean crack length (mm)	0.608 ± 0.034	0.559 ± 0.237	0.897 ± 0.275	0.395 ± 0.110	0.557 ± 0.101
Width of cracks (mm)	0.318 ± 0.051	0.339 ± 0.077	0.481 ± 0.095	0.190 ± 0.016	0.265 ± 0.055

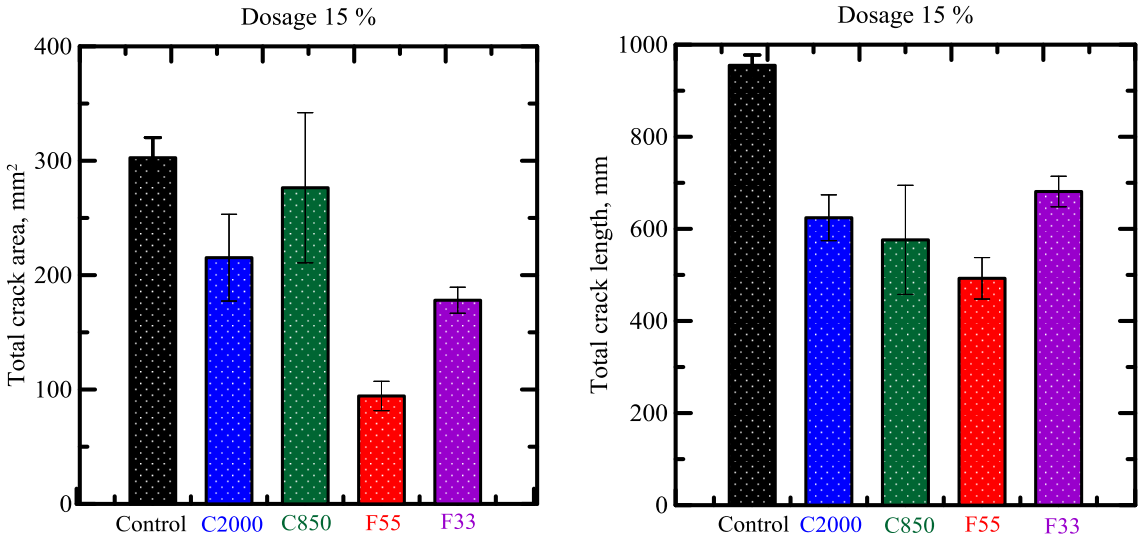

(a) (b)

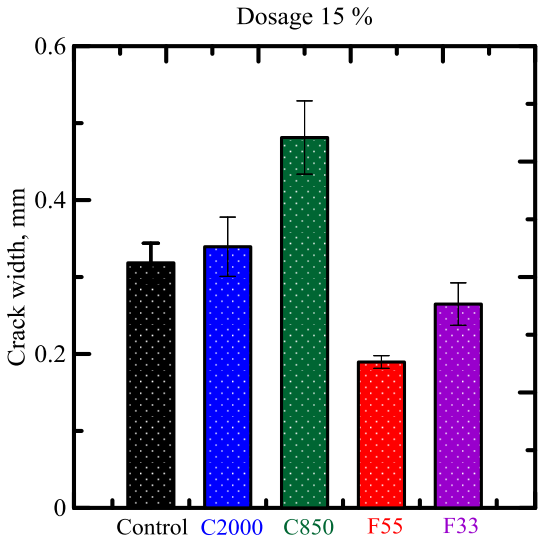

(c)

Figure 2.13 – Effect of Wollastonite in Altering Early Age Shrinkage in Wollastonite Cement Based Paste Specimens: a) total track area; b) total crack length; c) crack width

2.5.3 Sequential Crack Formation

Sequential crack formation was studied using crack quantification technique on the photographs of the specimens at different time intervals for the entire test duration. The summation of sequential crack formation is presented in Figure 2.14, wherein crack area with respect to time is shown. It can be observed from Figure 2.14 that the formation and growth of the cracks occurs in small time zone in the beginning of the test. The initiation of the crack is fairly consistent for the all of the specimens and is around two hours after the beginning of the test. The growth of the cracks is completed after approximately three hours. The amount of crack formation for the control specimens is much higher when compared to specimens which have cement replaced with wollastonite. Furthermore, the formation of cracks for control specimens is much more rapid within the three hour time zone. Replacement of cement paste with wollastonite nano-fibers significantly limits the area crack growth, but also decreases the rate at which

the crack area increases. Similarly to the trends observed in diffusion and evaporation, smaller sizes of wollastonite fiber have the most impact. F55 fiber provides the best results as it limits the crack area rate, defined as crack area change within the crack growth time zone, by an order of magnitude.

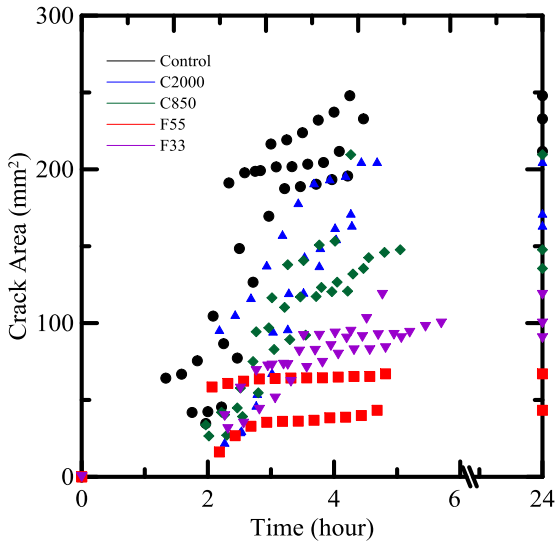

Figure 2.14 – Effect of Wollastonite in Sequential Crack Formation

The relationship between crack morphology and cumulative moisture loss was studied by comparing average cumulative moisture loss to average crack area at different time values. Figure 2.15 shows the results of such relationship. It is clear from Figure 2.14 that a higher value of crack area does not yield higher cumulative moisture loss which further supports the hypothesis of micro cracks responsible for higher evaporation rates, diffusivities and cumulative moisture loss.

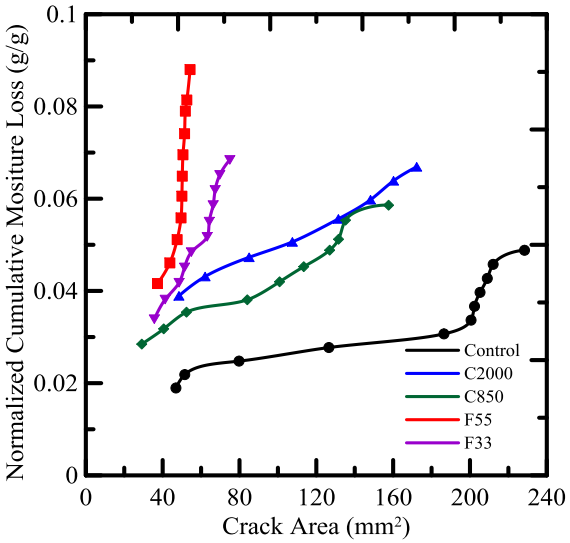

Figure 2.15 – Effect of Wollastonite in Cumulative Moisture Loss with Time

2.6 Pore Structure

2.6.1 Experimental Program

Mercury intrusion porosimetry (MIP), a common method of evaluating pore structures of cementitious materials [45,46,47], was used to study pore structure of the control and wollastonite specimens. A porosimeter that is capable of generating a pressure of 414 MPa to detect minimum pore size of 0.003 μm was used for this study. Testing procedure consisted of two steps. Step 1 involved evacuation of gases and filling the sample holder with mercury. Low pressure step is then used to increase the pressure to 345 kPa. Step 2 consisted of mercury instruction into the sample at high pressure up to 414 MPa.

Control and one type of coarse and fine fibers, namely, C850 and F55, were selected for the test. Additionally, effect of vacuum drying on the pore structure of these composites was investigated by curing the control mix under normal curing conditions at 23º C and 100 % RH. To differentiate between the two controls used, control dried in the

curing room was labeled as “Control Normal”; control dried in the vacuum was labeled as “Control Vacuum”. After 24 hours of normal and vacuum drying, specimens were demolded and further air dried until the day of testing. All of the specimens were tested around 7 days after casting. Two replicates were tested for each type of specimens. Since the replicates of each specimen were almost identical, they are not presented herein.

2.6.2 Results and Discussion

The comparison between Control Vacuum and Control Normal is presented in Figure 2.16. It is clear from the Figure 2.16 that drying cement paste specimen using vacuum set-up introduces a larger quantity of smaller sized pours that are less distributed when compared to the conventional drying technique. Up to about 5 μm, volume intruded is dominated by the vacuum control specimen. Volume intruded 0.003 μm pore size is increased by roughly 43 %; total volume intruded of a pore size up to 5 μm is increased by 264 %. This can be justified with the pressure imposed from the vacuum on the specimen which causes change in the pore distribution.

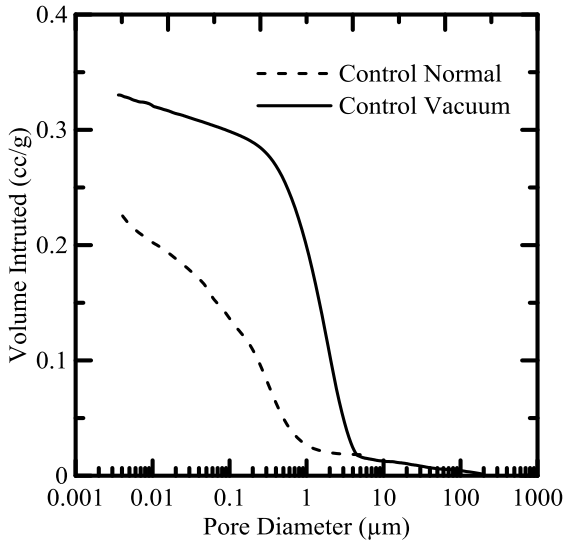

Figure 2.16 – MIP Results Comparison Between Control Vacuum and Control Normal

Figure 2.17 (a) provides a summary of the wollastonite fiber study, wherein volume intruded and pore size distribution is shown with respect to the pore size. It can be observed that the addition of wollastonite, depending on what size of fiber it is, adjusts the pores to an even smaller size. The coarser size fiber C850 is only slightly different in the 0.8 – 100 μm range, keeping the smaller pore sizes the same. However, the fine size fiber F55, introduces much smaller sized pores. This is reflected in an increase of 12 % of volume intruded at 0.003 μm pore, equivalent to 80 % additional volume intruded on the whole pore size curve. The benefits of wollastonite addition can also be noticed in the pore size distribution, Figure 2.17 (b), wherein critical pore size distribution is reduced by 23 % percent.

The results provided by the MIP testing can be used as a firm conformation of the crack reinforcement on the nano-level by wollastonite fibers. Due to the size and aspect ratio of the wollastonite, adding them into the cement-based mix produces small size inclusions that increase the amount of nano and micro pores present in the paste. Additionally, the amount of macro pores is reduced. Once the shrinkage process is initiated, the smaller size pores are the initial pores to collapse. However, the wollastonite fiber is able to provide reinforcement within the matrix and restrict the crack growth at nano level, thus, limiting crack development the macro scale. The effectiveness of wollastonite fiber against cracking is reflected in the fiber size, wherein smaller size fibers are more effective on the nano scale.

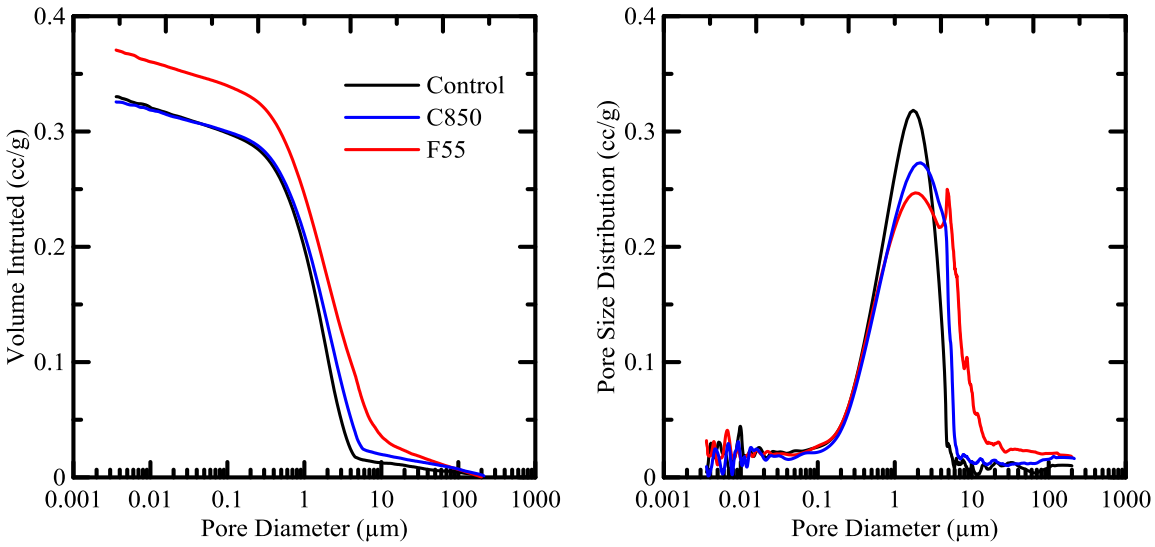

(a) (b)

Figure 2.17 – MIP Results on Wollastonite Study: a) volume intruded per pore diameter, b) pore size distribution per pore diameter

2.7 Conclusion

Early age two-dimensional plastic shrinkage cracks and diffusivity of wollastonite-cement based paste composites were studied under low-pressure vacuum condition. Analytical solution to boundary value problem of diffusivity and quantification of crack intensity using image analysis were employed to evaluate the performance of the composite. Wollastonite nano-fiber composites were compared on the basis of partial replacement of cement wherein four different wollastonite sizes (33 μm – 2000 μm) were used at 15 % replacement of cement content. The results of the study indicated that the nano-fiber composite inhibited increased initial evaporation rate, up to 40% and Stage II diffusivity, up to 14 %, when compared with a control specimens. Although cumulative moisture loss increased of up to 29 %, wollastonite nano-fibers provided an improvement to the all shrinkage cracking related parameters by restraining the crack growth at the

nano-level, reducing total length of cracks and crack width by a factor of two, and cracked area by as much a factor of three.

.

3. WOLLASTONITE-TEXTILE REINFORCED CEMENTITIOUS COMPOSITE

3.1 Introduction

In addition to fibres, there are other commonly used reinforcements which can be combined with plain paste/concrete to improve tensile properties. This type of reinforcement typically consists of different mesh configuration of steel bars or wire mesh. Although effective in many situations, such type of reinforcement is vulnerable to corrosion, which can weaken the concrete and amplify the damage done by shrinkage. In recent years of research a more innovative approach, targeting sustainability of reinforced concrete, allowed for the development of Textile Reinforced Concrete (TRC), which improves tensile, flexural and energy absorption properties of concrete [48,49,50]. Textile is defined as a flexible woven material which consists of network of yarns (threaded fibers). Generally, fiber materials used for textile development include: alkali-resistant glass (ARG), carbon, basalt, aramid and polyvinyl-alcohol (PVA) [50,51,52]. In addition to strength gains, usage of textile as the reinforcement medium can reduce usage of Portland cement, therefore, creating many different areas of avenues in structural applications.

Textiles are characterized by an open grid structure with interwoven yarns perpendicularly to each other. They are particularly well suited for a bi-axial case of loading. Addition of textile can provide an increased surface area to which cement paste can bond and act as a reinforcing medium. Such reinforcement can potentially promote distribution of the applied stress evenly throughout the exposed surface area of the specimen, thus avoiding stress concentrations. Textiles can also be potentially used as a

reinforcing medium against shrinkage cracking with minimal effort. Moreover, a combination of wollastonite and textile reinforcement could produce an improved hybrid reinforcing medium, wherein a new shrinkage restricting mechanisms can emerge. The combination of stress distribution leading to distributed cracking mechanism due to the presence of textiles and fibers bridging and deflection of the crack path can promote better crack restriction and an improved surface of the specimens. In this part of the thesis, the behaviour of textile-wollastonite hybrid reinforcement is investigated for their role in shrinkage resistance, using the techniques discussed in the initial chapters.

3.2 Experimental Program

The experimental program consisted of evaluating four different types of wollastonite fibers, two coarse sizes of HARRP and two fine sizes of NYAD-G. In addition to wollastonite, the specimens were reinforced with one layer of a precut patch of ARG textile. Figure 3.1 shows the positioning of the textile in the mold. The textile was inserted into the mold and connected to the mold by the means of hooks that secured the textile from any movement during the paste pouring. Fixing the textile to the mold also prevented any movement during the testing while the pressure is exerted on the specimen surface. As previously done, corresponding specimens are herein referred to by the sizes of wollastonite fibers of 2000 μm, 850 μm, 55 μm and 33 μm as TC2000, TC850, TF55, TF33, respectively. Letter "T" is used to differentiate specimens that are only reinforced by wollastonite with specimens that are additionally reinforced with textile. Other the mixing materials, such as Portland cement and water reducing admixtures, as well as the mixing procedure, are identical to those presented in the previous chapter were used for the textile testing

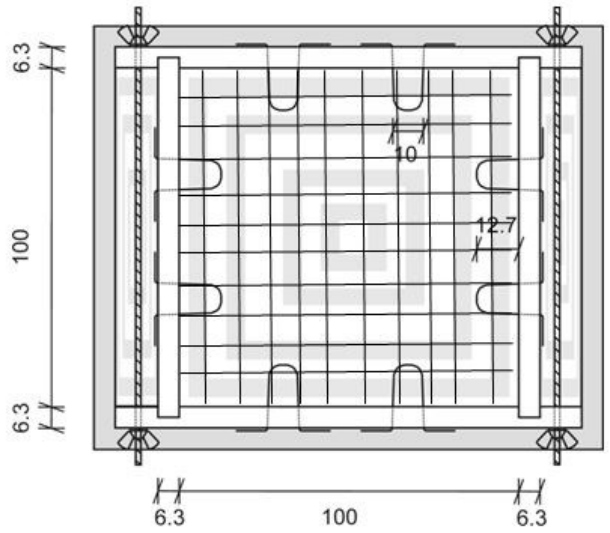

Figure 3.1 - Plan View of the Mold with the Textile Reinforcement (numbers in mm) [33]

3.3 Results and Discussion

3.3.1 Evaporation

The effect of wollastonite nano fibers, as an additive to textile reinforcement, in restraining the growth of early age shrinkage cracks of cement-based paste specimens was studied using the drying and evaporation response as presented in Figure 3.2. Specimens are compared on the basis of fiber type (size) in the presence of ARG textile. As evident, the behavior of the specimens is quite similar with respect to both moisture loss and evaporation rates. Parameters that characterize the drying response of these composites which include evaporation rates, transition time between Stage I and Stage II, diffusivity of Stage I and Stage II and cumulative moisture loss are reported in Table 3.1; accuracy of the fitting model is reported. The average value recorded from testing of minimum three replicate specimens from each testing group is summarized along with the associated standard deviation.

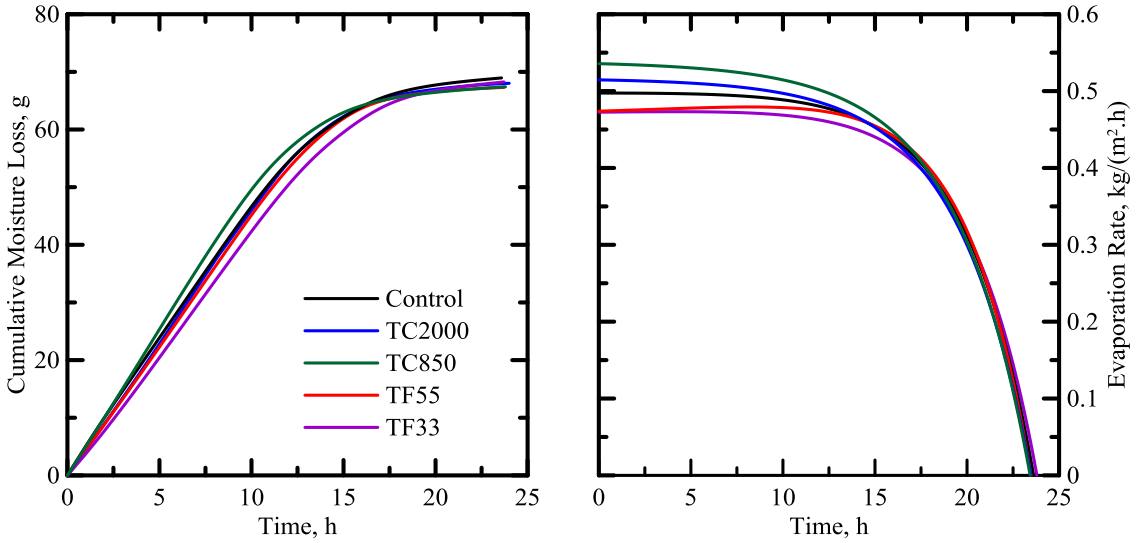

(a) (b)

Figure 3.2 – Effect of Textile and Wollastonite Addition on Evaporation Tests Results: a) cumulative moisture loss, b) evaporation rate

Table 3.1 – Drying Parameters Summary of Textile-Wollastonite Specimens

Specimen Type	Initial Evap. Rate (kg/(m^{2}h))	Cumulative Moisture Loss at 24 h (g)	Transition Time (h)	Diffusivity Stage I (m^2/s)	Diffusivity Stage II (m^2/s)	Prediction Accuracy (%)
TControl	0.479 ± 0.036	66 ± 1	9 ± 1	1.85E-3	2.69E-4 ± 2.02E-5	97 ± 3
TC2000	0.505 ± 0.045	69 ± 3	9 ± 1	1.85E-3	2.45E-4 ± 1.16E-5	97 ± 1
TC850	0.510 ± 0.010	69 ± 1	9 ± 1	1.85E-3	2.46E-4 ± 1.89E-5	99 ± 0
TF55	0.469 ± 0.070	69 ± 5	10 ± 2	1.85E-3	2.44E-4 ± 1.71E-5	98 ± 2
TF33	0.480 ± 0.085	69 ± 3	10 ± 1	1.85E-3	2.46E-4 ± 2.31E-5	99 ± 1

Effect of w/c ratio

The estimated cumulative moisture loss for control specimen reinforced with textile was found to be 0.191 and TRC specimens reinforced with 15% wollastonite

fibers of type: TC2000, TC850, TF55 and TF33 specimens was about 0.235 as g/g normalized w.r.t to the starting weight of paste specimen respectively. It is clear that specimens with higher w/c ratios yield higher cumulative moisture loss [40]. Cement replacement by wollastonite allowed for slightly higher w/c ratio as compared to control samples resulting in a 24% increase in the cumulative moisture loss. However, it is an interesting observation that for all four different types of wollastonite fibers, in the presence of textile reinforcement, have yielded the same amount of moisture loss. Higher cumulative moisture loss can be also measured through the Stage I and Stage II diffusivities reported. Stage I diffusivities were quite similar for all specimens; they are closely related to the diffusivity rate for plain cement paste at vacuum pressure. A decrease in diffusivity up to 9% for specimens reinforced with textile and wollastonite fibers is observed during Stage II. Decreased Stage II diffusivity is balanced through a 20 % increase in the initial evaporation rates for textile wollastonite specimens, contribution of which can have an effect on the increase in the cumulative moisture loss when compared to the control mix.

Effect of fiber type

Replacement of cement with wollastonite fibers, in addition to the textile reinforcement, resulted in a gradual transition between the modes of drying. No significant effect of cement replacement with wollastonite nano-fibers can be observed in the Stage I to Stage II transition time. Transition time for coarse fibers was not altered at all; however, transition time was increased by roughly by one hour for the finer sizes. Comparison of the initial evaporation rate and diffusivities based upon the type of wollastonite replacement indicates very small change. According to Figure 3.3(a),

diffusivity of Stage I and Stage II remains almost the same for all of the specimens; a decrease of 9 % can be observed when the specimens are compared to the control. Potential mechanism could be attributed to the textile providing heavy reinforcement and higher surface area to which cement particles can bond to, resulting in restriction of the crack width on the macro scale. As observed previously, wollastonite fiber can control the width of the crack on the nano scale. Therefore, the combination of the two types of reinforcements provides an improved form of reinforcement.

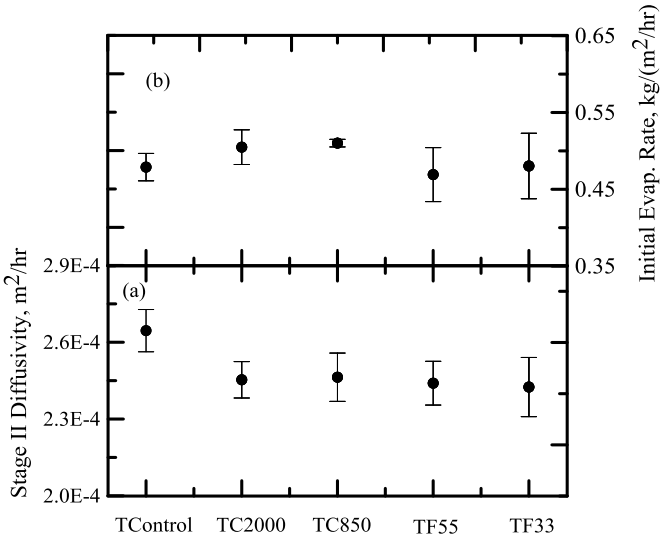

Figure 3.3 – Effect of Textile and Wollastonite Addition on Stage II Diffusivities and Initial Evaporation Rate

Similar to diffusivities, initial evaporation rate was also not greatly affected by the size of wollastonite fibers. Coarse and fine sizes of wollastonite yielded the same evaporation rate when compared to the control specimen as shown in Figure 3.3(b). In addition to higher w/c ratio and size of wollastonite inclusions, observed previously, mechanism controlling the evaporation could be also altered by the presence of the textile. Since during the Stage II, diffusivity occurs under internal mass transfer control, the microstructure plays a significant role in the drying process. Specimens reinforced

with textile and wollastonite exhibits slightly lower diffusivity as the microstructure does not allow for moisture to travel through the less cracked surface area. The ability of wollastonite to arrest cracks at micro level has a synergistic effect on the surface of the specimens as the textile limits the cracks on the macro-level that makes the specimen denser, thus, decreasing Stage II diffusivity. However, a slight increase in initial evaporation rate and longer transition time results in higher cumulative moisture loss in textile-wollastonite reinforced specimens.

3.3.2 Crack Morphology

Figure 3.4 (a-e) provides the scanned images of the representative specimens used for the crack morphology study. It is clearly evident that the addition of wollastonite fibers to the textile reinforcement is very effective in restraining the growth of shrinkage crack on the surface of the specimens when compared to the control mix. Textile enables a reinforcement mechanism which introduces cracks with much smaller width; however they increase the total crack length. As discussed in the last chapter, wollastonite fibers are effective in reducing early-age plastic shrinkage cracks. Thus, offering a coupling effect of reduced crack width from the textile aids in arresting the crack growth. In line with the discussions in the previous chapter, finer wollastonite fibers namely F55 and F33 are more effective in bridging the cracks at the nano-level. Thus due to coupled effect of textile reinforcement, combination of finer wollastonite fibers and textile are very effective in reducing the extent of cracks at the macro level. Again, this could be accredited to the uniform dispersion of the smaller size nano-fibers across the cementitious matrix, which allows for the potential of efficient blending with the paste matrix, producing very good coupled reinforcement.

Analyzed crack morphology results have been summarized in Table 3.2. Total area of cracks, crack length and width has been considered to compare different groups of specimen. Figure 3.5 summarizes the effect of different wollastonite fiber types in controlling the growth of shrinkage cracks evaluated in the current study. As evident there is substantial reduction in most shrinkage cracking related parameters for all specimens reinforced with textile and wollastonite, when compared to textile control paste specimens.

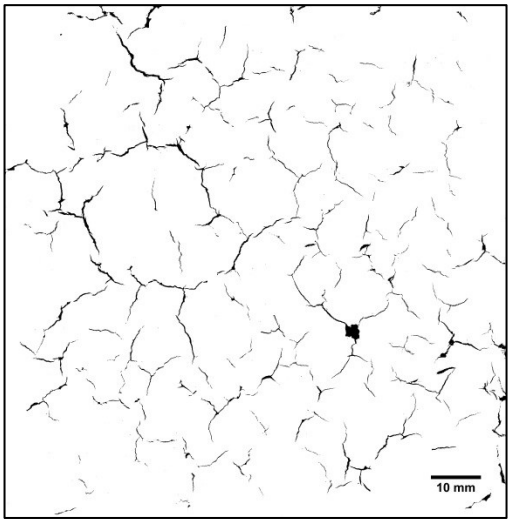

(a) TControl Paste

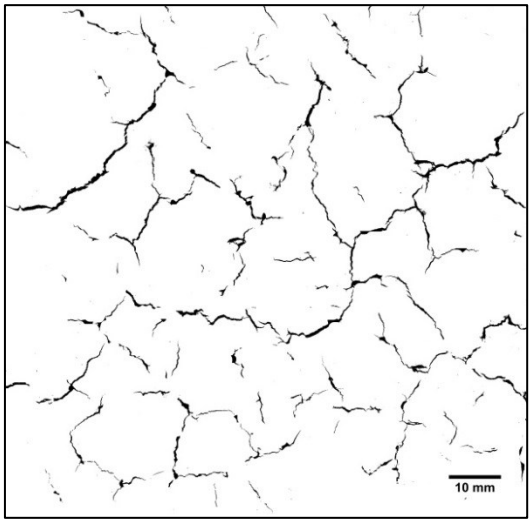

(b) TC2000 Paste

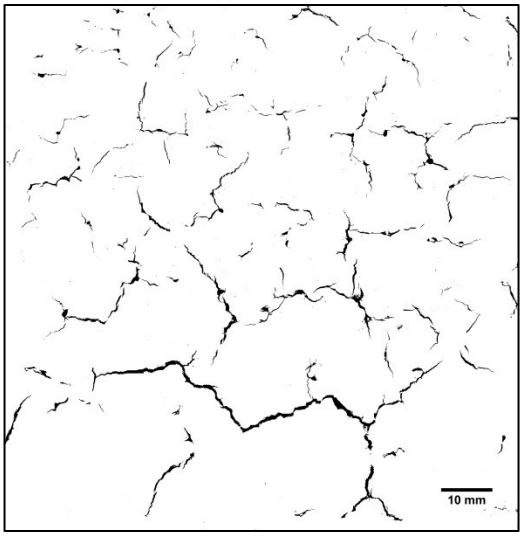

(c) TC850 Paste

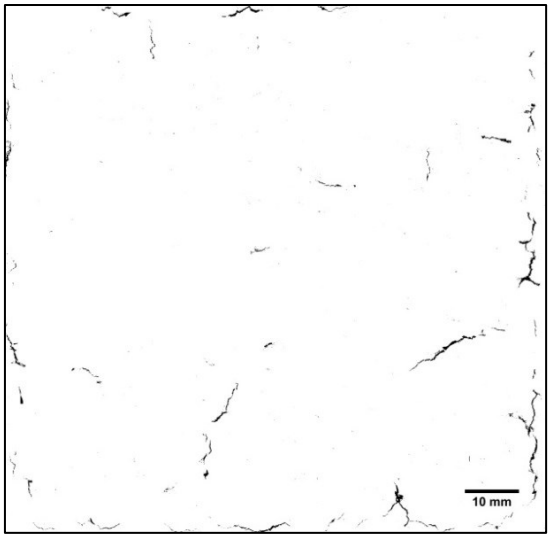

(d) TF55 Paste

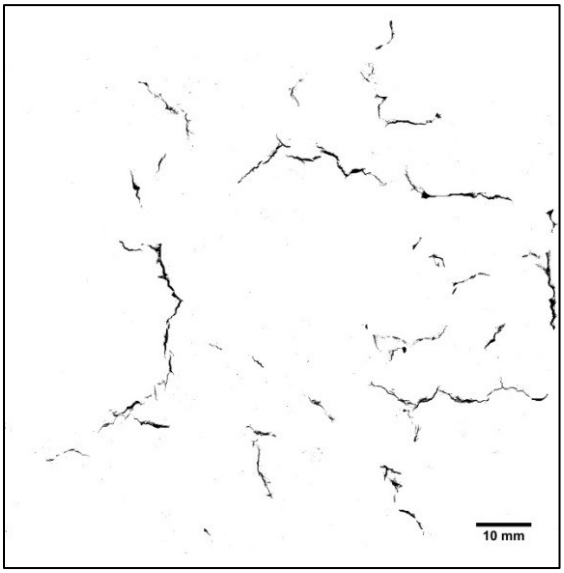

(e) TF33 Paste

Figure 3.4(a)-(e) - Cleaned Up Binary Images of representative Textile-Wollastonite Specimens

It is to be noted that the efficiency of wollastonite fibers can be related to the relative reduction in the magnitude of cracking parameters. Amongst all four grades of wollastonite, F55 is most effective in improving resistance to early-age shrinkage cracks. Total crack length, width and area is reduced by as much a factor 5, 1.5 and 8, respective,

for specimen's reinforced textile and F55 wollastonite fiber when compared to control textile specimens. It is also evident that the remaining forms of wollastonite fibers are marginally better in limiting the growth of shrinkage cracks. For instance, TC2000 fibers can reduce the total crack length by 4 %, but increase cracked area by 20 %. TC850 fibers increase the width of cracks by 10 % and the crack area by about 2 %. The phenomena can be related to the coarse size nature of the fiber as the arrest of the crack is initiated at a larger scale. Limiting the crack length produces wider crack causing higher cracked area. However, finer size fiber, TF33, can reduce the length of the cracks by 44 % and width of the cracks by 15 %. Cracked area can also be reduced by 51 % with TF33 fibers.

Table 3.2 – Crack Morphology Summary of Textile-Wollastonite Specimens

Crack Properties	**TControl**	**TC2000**	**TC850**	**TF55**	**TF33**
Length of cracks (mm)	1037 ± 241	993 ± 123	935 ± 45	201 ± 137	585 ± 44
Area of cracks (mm^2)	200 ± 33	248 ± 35	204 ± 7	25 ± 19	93 ± 1
Density of cracks (mm^{-1})	0.104 ± 0.024	0.099 ± 0.012	0.094 ± 0.005	0.020 ± 0.014	0.058 ± 0.004
Mean crack length (mm)	0.584 ± 0.054	0.581 ± 0.075	0.540 ± 0.088	0.162 ± 0.024	0.277 ± 0.041
Width of cracks (mm)	0.199 ± 0.078	0.250 ± 0.005	0.218 ± 0.009	0.119 ± 0.011	0.159 ± 0.021

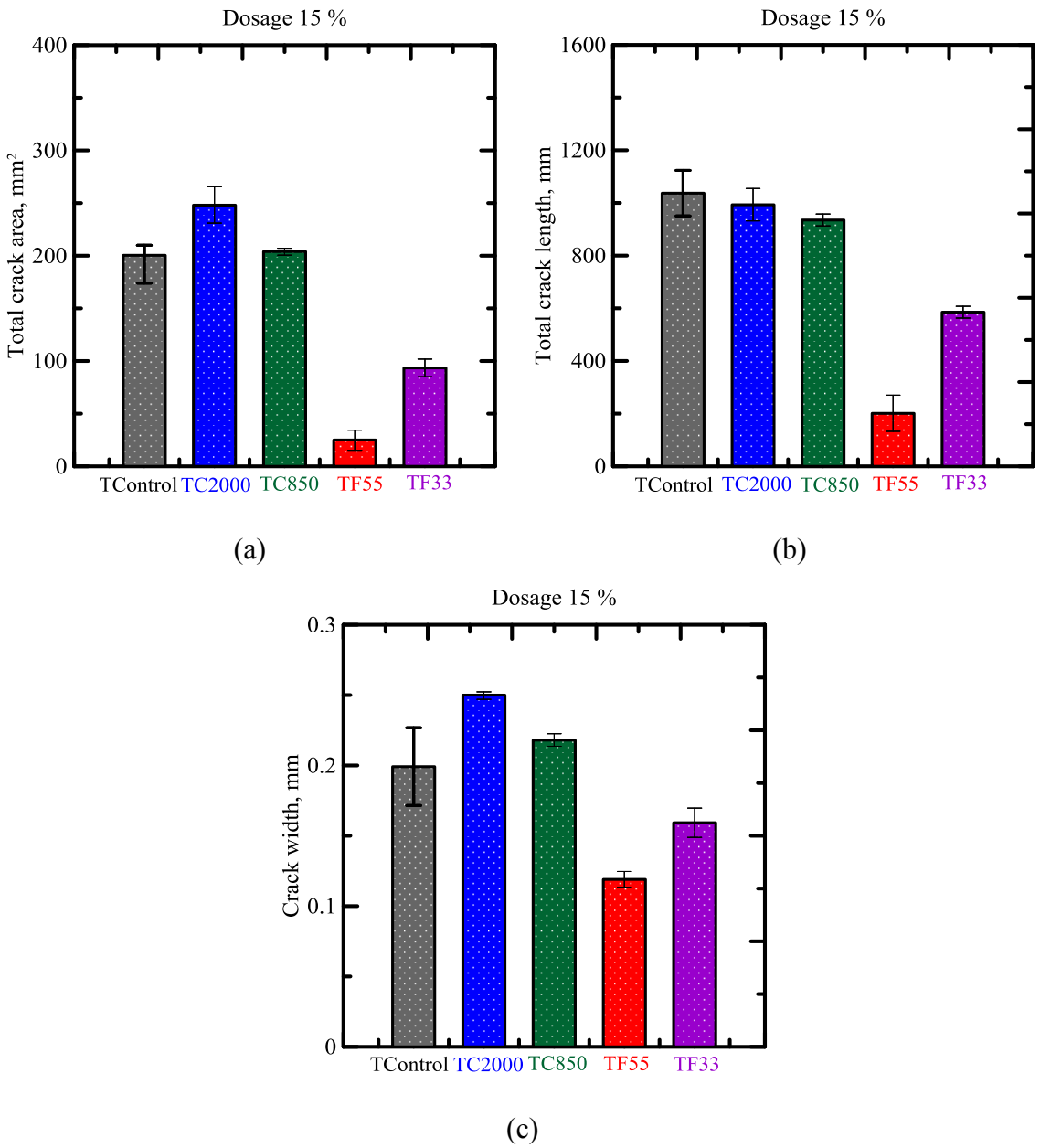

Figure 3.5 – Effect of Textile and Wollastonite in Altering Early Age Shrinkage in Cement Based Paste Specimens: a) total track area; b) total crack length; c) crack width

3.3.3 Sequential Crack Formation

Propagation of cracks on the exposed surface of the specimen was studied using crack quantification techniques on the photographs of the specimens at different time

intervals for the whole test duration. Time history of total crack area is presented in Figure 3.6.

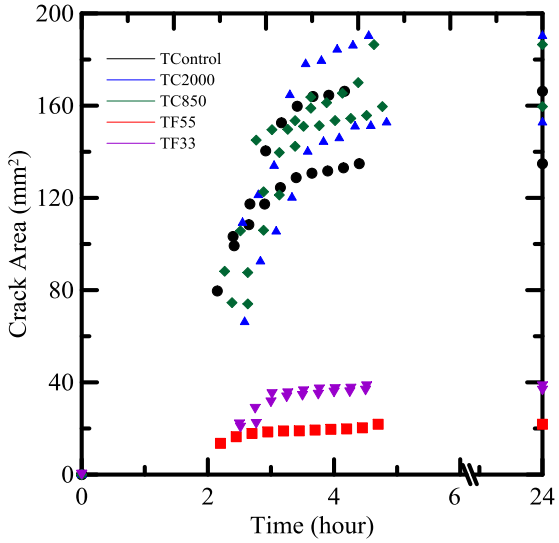

Figure 3.6 – Effect of Textile and Wollastonite in Sequential Crack Formation

It is evident that the formation and growth of the cracks occurred in small time zone in the beginning of the test. The initiation of the crack is fairly consistent for the all of the specimens and is around two hours after the beginning of the test. The growth of the cracks is completed roughly three hours later. This observation is consistent with the results obtained for wollastonite shrinkage testing and can suggests that crack initiation is independent of the reinforcement type. The amount of crack formation for the control textile specimens is very similar to the specimens with textile and coarse fibers. However, the difference is much more apparent for the specimens with combination of finer fibers and one layer of ARG textile. The formation of cracks for TControl, TC2000 and TC850 specimens is much more rapid within the three hour crack growth time zone; it is very similar with respect to each other. Replacement of cement paste with textile and finer wollastonite nano-fibers significantly limits the area crack growth, but also

decreases the rate at which the crack area increases. Combination of ARG textile F55 fiber provides the best results as it limits average the crack area rate, defined as crack area change within the crack growth time zone, by an order of magnitude.

The relationship between crack morphology and cumulative moisture loss was studied by comparing average cumulative moisture loss to average crack area at different time steps; and is presented in Figure 3.7. As evident, finer wollastonites fiber in a presence of textile produce higher cumulative moisture loss at lower cracked area, whereas the combination of coarse size fiber and ARG textile produces higher cumulative moisture loss, and much higher cracked area.

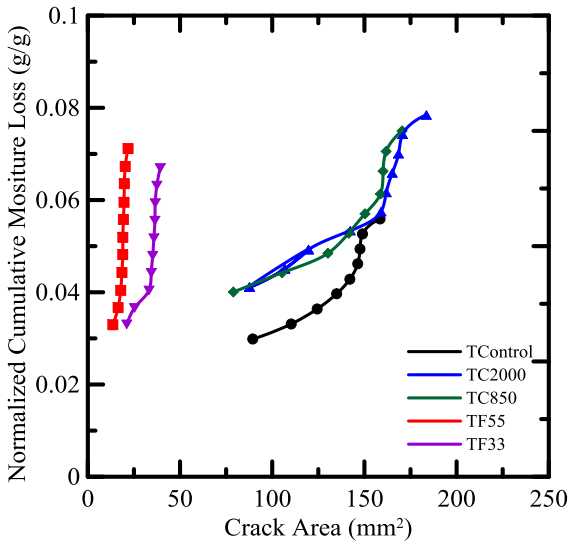

Figure 3.7 – Effect of Textile and Wollastonite in Cumulative Moisture Loss with Time

3.4 Effect of Textile Reinforcement in Shrinkage Properties

Comparison between the only wollastonite and textile-wollastonite hybrid reinforcement is discussed in the following section. Results obtained from the two sets of tests including diffusion simulation and crack morphology are used for discussion purposes.

3.4.1 Drying Properties

The difference in the normalized cumulative moisture loss for the two different sets of specimens is presented in Figure 3.8, wherein average values are shown with error bars. From Figure 3.8, it can be observed that moisture loss for control with textile is increased by 1.5 %. Such a small change can be considered a variation within the experiment set-up or the analysis procedure. However, moisture loss is almost the same for all of the textile-wollastonite reinforced specimens when compared to specimen reinforced only with wollastonite; small variations are observed depending of the size of the fiber. The differences can be further observed in the initial evaporation rates and Stage II diffusivities, which decrease by about 16 % and 13 %, respectively. These changes are evident in Figure 3.9. Currently, there's no explanation why the textile wollastonite reinforced specimen have lower diffusivity and evaporation values, but yet yield almost the same cumulative moisture loss when compared to wollastonite reinforced specimen. The reasons may arise from the choice of the analytical techniques employed wherein more simplified assumptions are used. Further testing and more advanced modeling techniques may provide more insight in differentiating wollastonite and textile-wollastonite reinforcement. Based upon the results obtained from the comparison of the two types of reinforcement regarding drying properties, it can be concluded that the changes are small enough to be negligible.

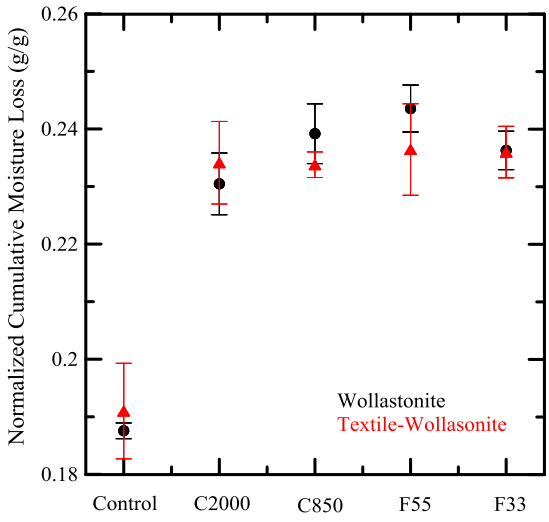

Figure 3.8 – Comparison of Normalized Cumulative Moisture Loss for Two Different Types of Reinforcement

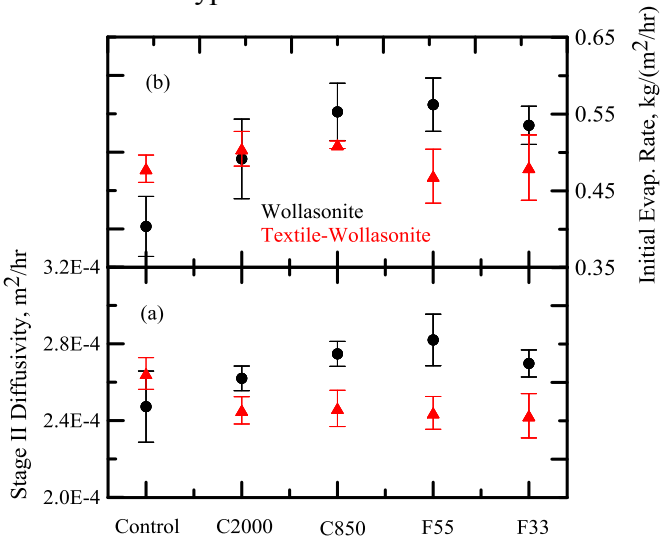

Figure 3.9 – Comparison of Stage II Diffusivity and Initial Evaporation Rate for Two Different Types of Reinforcement

3.4.2 Cracked Surface

Figure 3.10 is presented to provide visual difference between the surface texture of wollastonite reinforced and textile-wollastonite reinforced specimens. It is evident that specimens with one layer of ARG textile produces less cracked area, therefore, providing better reinforcement. While comparing the crack quantification parameters, interesting

results can be seen. For instance, while comparing the presence of the textile, control with textiles has an increase of crack length by 9 %; however, there is a 34 % reduction in crack area due to the crack width reduction of 37 %. When comparing TC2000/TC850 with C2000/C850, a reduction in crack width is reduced for up to 54 % facilitates an increase in the cracked area of the specimens by up to 63 %. This type of cracked surface is different from what was previously observed with wollastonite only reinforced specimens. Such behavior can be accredited to the size of the fiber. Since C2000 and C850 fibers are the coarser fibers, the effectiveness of the fiber on the nano-scale is less than that of a smaller size fiber such as TF55 and TF33. In combination with the mechanism of increase crack length and reduced crack width that is offered by the textile, the coarse size fibers are not able to bridge the micro-cracks and thus affecting the overall performance of the composite.

TF55 and TF33 specimens follow a very similar pattern as observed with F55 and F33 specimens, wherein all the morphological parameters are vastly reduced. The reduction of the crack parameters brings additional improvement to the surface of the textile reinforced specimens. This is reflected in additional decrease of 37 %, 59 % and 73 % for TF55 specimen in crack width, length and area respectively; TF33 specimen has additional decrease of 14 %, 48 % and 39 % in crack width, length and area, respectively. Figure 3.11 summarizes the comparison between the two data sets. Similar argument can be made towards the effectiveness of the finer size fibers. The ability of the fiber to blend in effectively with the cement paste offers much better crack restraint on nano-scale. In combination with the textile reinforcement mechanism, provide an excellent composite reinforcement of the specimen.

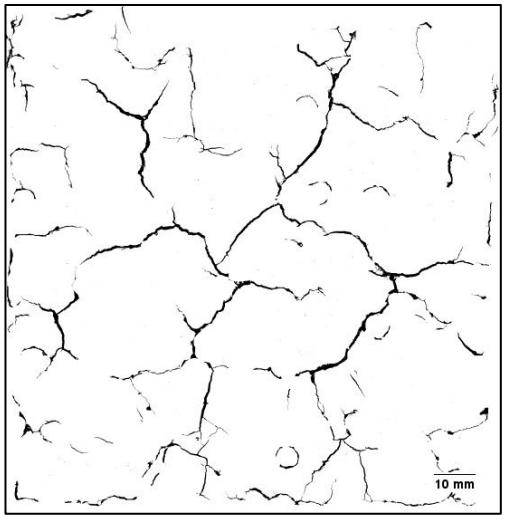

Control

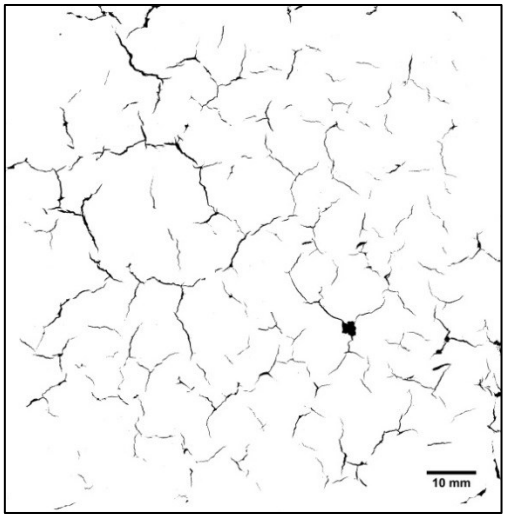

TControl

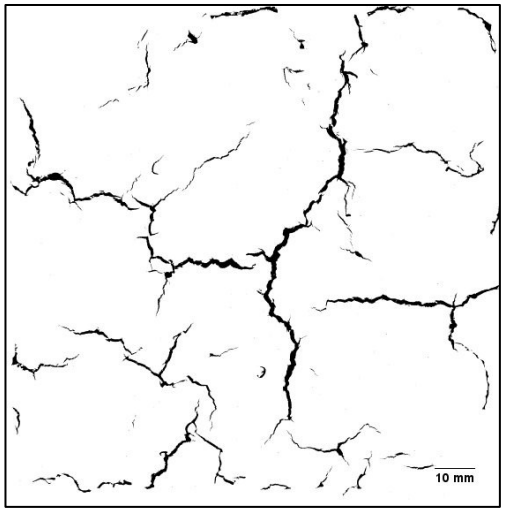

C2000

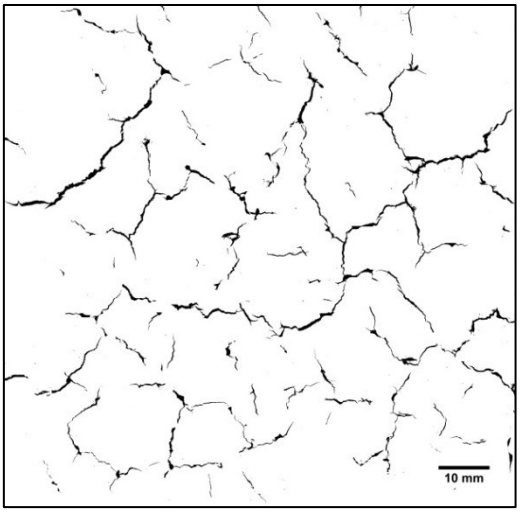

TC2000

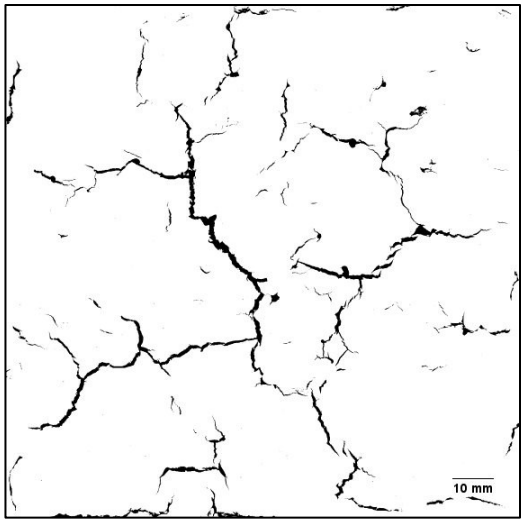

C850

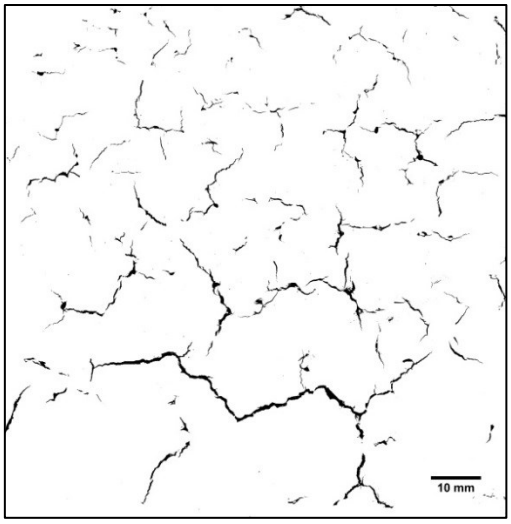

TC850

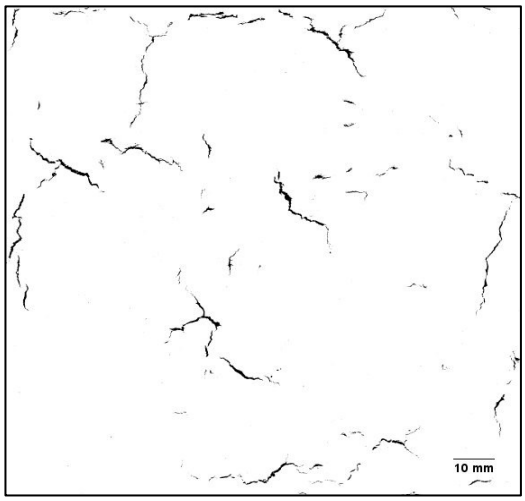

F55

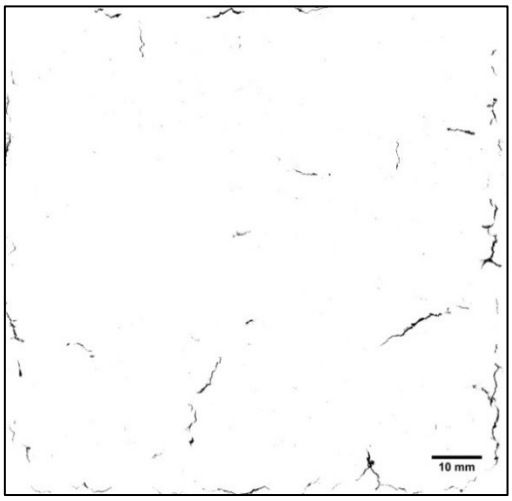

TF55

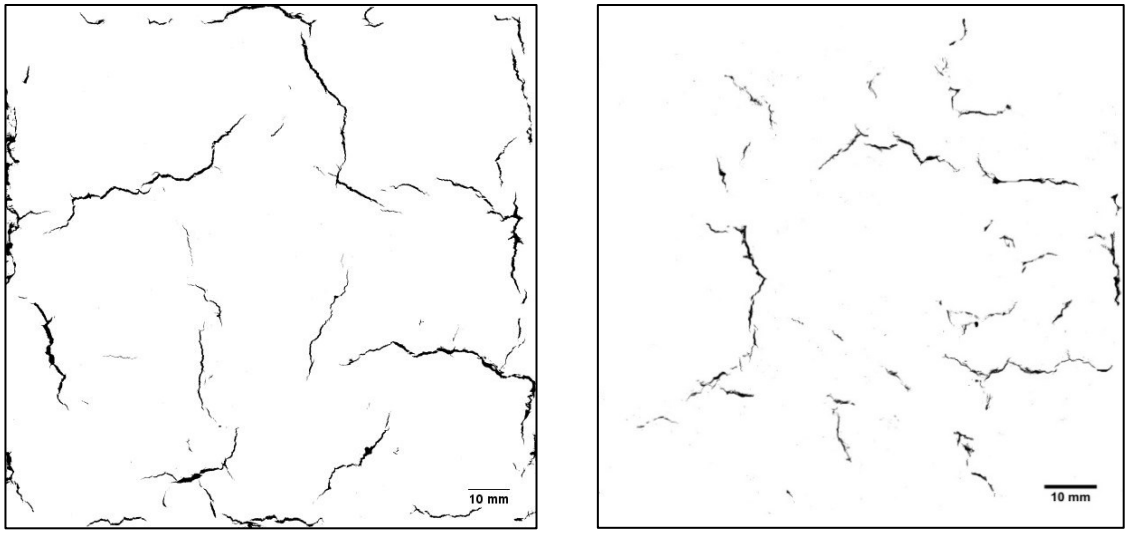

F33 TF33

Figure 3.10 – Visual Comparison of Crack Morphology for Wollasonite and Textile-Wollastonite Specimens

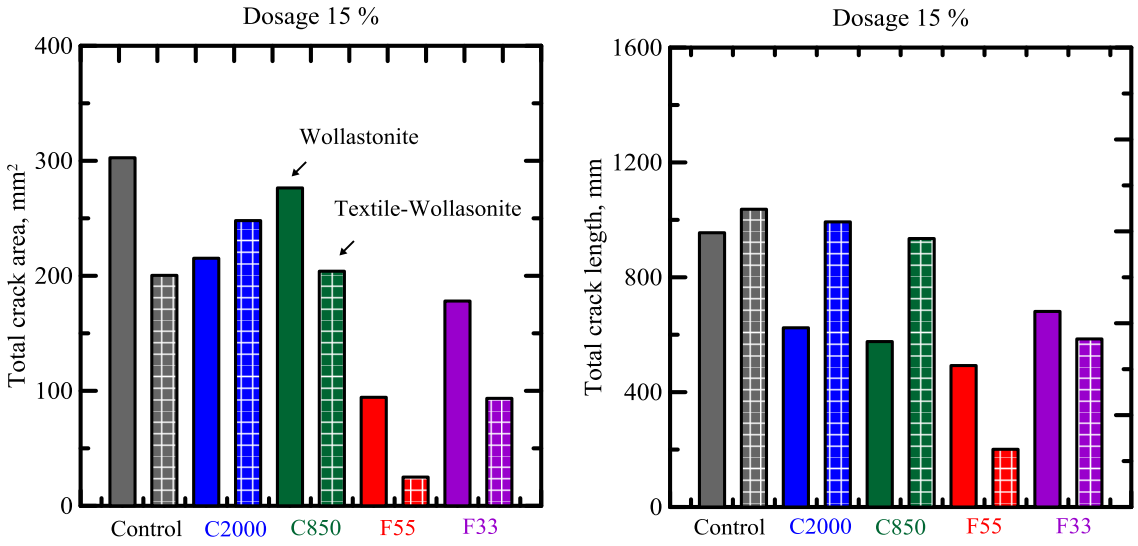

(a) (b)

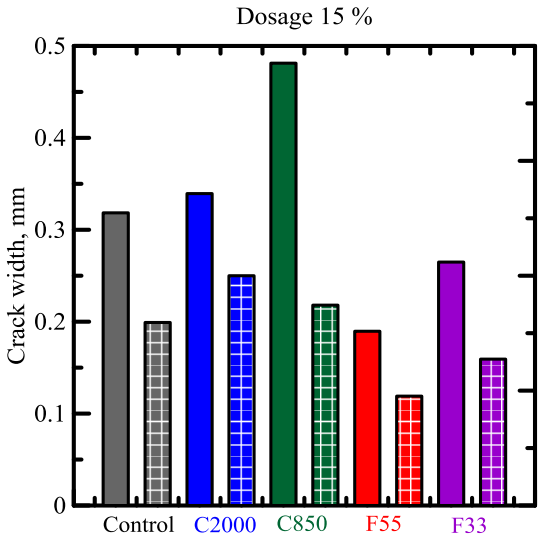

(c)

Figure 3.11 – Crack Morphology Comparison of Wollastonite and Textile-Wollastonite Specimens: a) total track area; b) total crack length; c) crack width

To showcase the outstanding performance of the textile-wollastonite composite it is herein compared to plain control specimens. The synergistic effect of the textile and wollastonite reinforcement improves the tensile strength of the paste matrix dramatically. In the presence of the textile reinforcement, F55 fiber decreases crack length by 79 %, crack width by 63 % and crack area by 92 % when compared to the plain control specimens.

3.4.3 Sequential Crack Formation

Comparison of sequential crack formation between the two types of reinforcement shows rather similar trends. Specimens reinforced with wollastonite only show a specific trend of crack formation reduction with the decreased fiber size; the transition from control to F55 and F33 is smooth. However, when textile-wollastonite specimens are compared on such basis, difference is much more noticeable. The crack formation of coarse size fibers is almost the same as for control. Also, the transition between from

control to fine size fibers shows a drastic jump. However, due to the presence of textile, the amount of cracking is limited. These relationships can be observed in Figure 3.12, wherein the reinforcements are compared side by side.

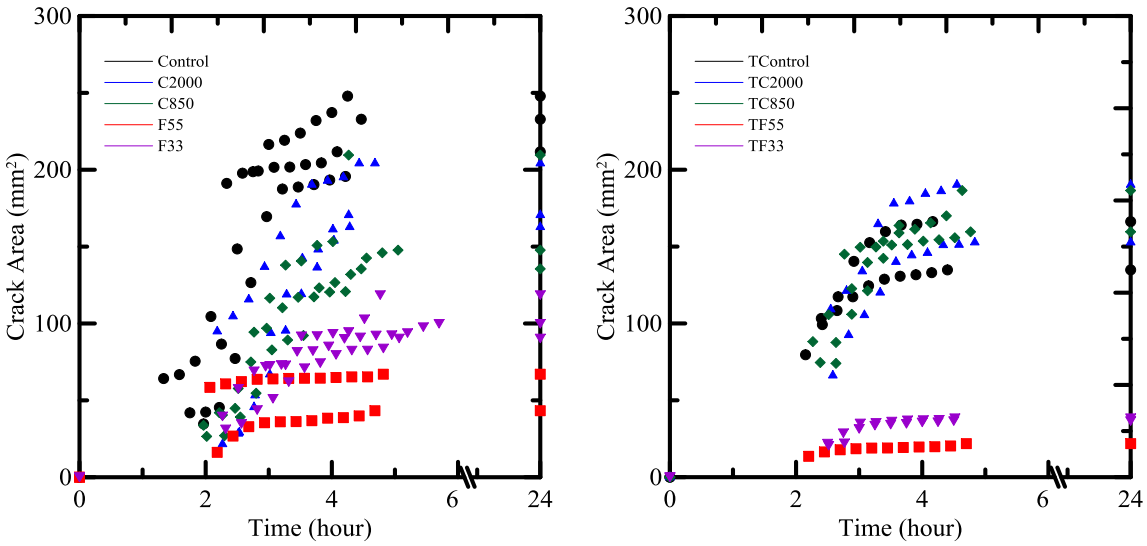

Figure 3.12 – Sequential Crack Formation Comparison of the Two Types of Reinforcement: a) wollastonite, b) textile and wollastonite

Comparison in the cumulative moisture loss with development of cracks in time is shown in Figure 3.13. Similar trends are observed for the fine size fibers, wherein in small amount cracked area yield higher normalized cumulative moisture. However, it should be noted that for textile-wollastonite specimens, due to the presence of the textile, final normalized cumulative moisture loss with coarse fibers is the same as finer fibers. Thus, suggesting that in the presence of textile, coarse size fibers may a different mechanism for the moisture loss.

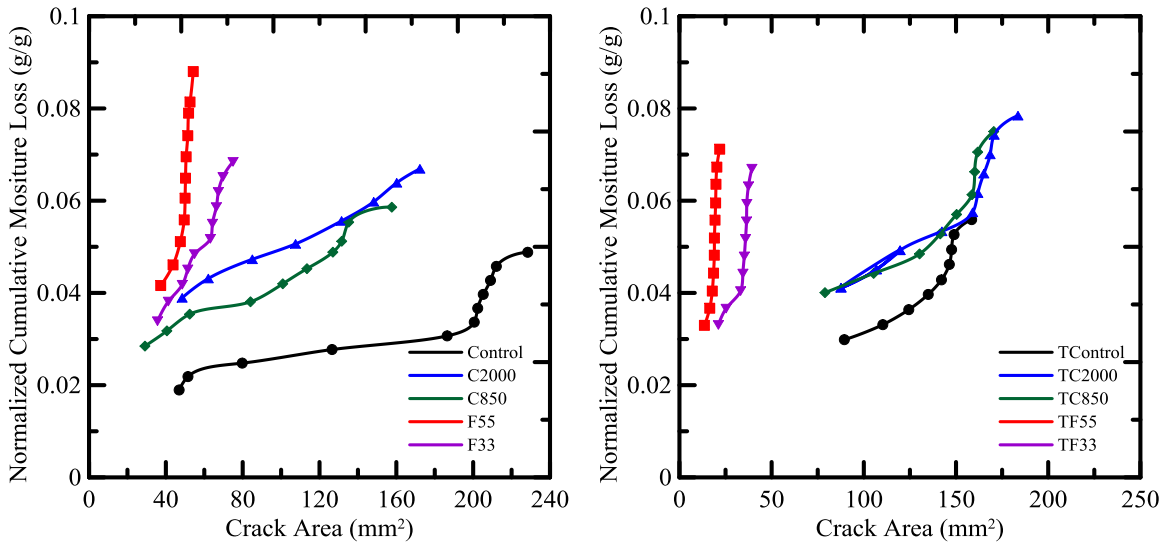

(a) (b)

Figure 3.13 – Cumulative Moisture Loss with Time Comparison of the Two Types of Reinforcement: a) wollastonite, b) textile and wollastonite

3.5 Conclusion

It has been shown throughout this work that textile, as a standalone material, can be used in plastic shrinkage control, by distributing the tensile stress over the surface area of the specimen. The drying and crack morphology of the specimens with one layer of AR-glass textile and wollastonite fibers were studied for their shrinkage resistance under low pressure vacuum conditions. It was observed that textile reinforcement produces mechanism that distributes tensile stress, induced from the shrinkage, producing distributed cracks with limited width. The results obtained from the analysis showed that combination of textile and wollastonite as reinforcement had negligible changes in the drying properties, but decreased the total cracking area of the specimen drastically. Combination of ARG textile with F55 wollastonite fiber produces specimen surface area that had reduction of 37 % in crack width, 59 % in crack length and 73 % in total crack

area. This can be explained in terms of the finer wollastonite fibers being effective in arresting the crack at nano-scale, and ARG textiles limiting the growth of cracks on the macro level. The combination of the two mechanisms produces a style of reinforcement that is very effective in restraining the growth of shrinkage cracks.

.

4. DEVELOPMENT OF LARGE SHRIKAGE TESTING

4.1 Introduction

As a part of advancement of simulating drying properties of cement, specimen size and constituent matrix materials are important factors. Naturally, such issues can be addressed by producing larger size specimens and different types of constituents to produce the material desired. The first two chapter of this work showed and discussed drying and crack morphology properties of cement paste in combination with wollasonite and textiles. The work presented within this chapter introduces the difficulties in manufacturing a larger shrinkage set-up wherein drying and crack morphology studies can be conducted. The main objective of the study consisted of producing consistently cracked specimen surface area with drying properties similar to the results obtained for 100x100x14 mm paste specimens, discussed in the earlier chapters. Drying concepts and image analysis presented in the first chapter were applied to study the behavior of large scale specimens; correlation with the smaller size paste specimens was made.

The study conducted attempts to determine reinforcement style suited for simulation of random shrinkage cracking under low vacuum condition in concrete. Observation and discussion on specimen size increase and modified specimen composition are presented herein. Several different testing parameters were investigated during the study. These include type, positioning, depth and fixity of the reinforcement. Reinforcements were evaluated based upon the material, easy of build and assembly with the mold. The ability of the reinforcement to produce cracking was studied as a function of the material, wherein material composition was varied from paste to mortar, to

concrete formulations. Details of the different aspects as well as the results of the experiments are discussed in the following sections.

4.2 Testing Equipment Development

4.2.1 Chamber

Due to the increase in specimen/mold size, the vacuum chamber had to be increased in size. The original shrinkage chamber used previously consisted of a glass desiccator topped with clear polycarbonate lid. The volume of the old chamber was measured to be 2.91×10^7 mm^3 (1779 in^3). The new chamber was manufactured from steel to provide strength requirements due to the increased size. The previously attempted chamber, made out of thin sheet metal, buckled under the pressure from the pump, therefore thicker steel was decided upon to provide safety to the chamber and users of the equipment. The volume of the new steel chamber was measured to be 6.67×10^7 mm^3 (4072 in^3), about two times the size of the glass chamber used earlier in this study. 305 mm (12") diameter pipe with thickness of 9.53 mm (3/8") was used for the body of the chamber with a plate 6.35 mm (1/4") welded to the bottom. After a few initial test runs vacuum did not produce enough pressure build up inside the chamber, so silicon sealant was used outside and inside the chamber to eliminate any potential leakage. The chamber was topped with a custom neon-rubber gasket with a larger 13 mm (0.5") thick clear polycarbonate lid. Unlike the previous set-up, no vacuum grease was needed for the lid, as the new gasket gave vacuum proof sealing. The lid was modified with holes for the load-cell wiring and vacuum hose fitting; old parts were reused from the previous set-up. Photographs of the chamber are presented in Figure 4.1.

(a) (b)

Figure 4.1 – New Shrinkage Chamber: a) plan view, b) x-s view

4.2.2 Mold

Several different mold designs were considered. After a few basic sketches, the design of the current mold was finalized. The mold consisted of a square, 178x178 mm (7”x7”), base with rectangular sides. Two different lengths, 178x89 mm (7”x3.5”) and 203x89 mm (8”x3.5”), were used for the side walls as to provide an interlocking mechanism amongst all the sides. The sides were initially attached to the base and then attached to each other as to provide firm buildup of the mold. Two screws per side were used to attach the walls to the base plate; one screw was used to restrain the walls of the mold. Figure 4.2 shows geometric configuration of the mold.

The mold was manufactured out of wood due to the ease in operation and availability of the material and low fabrication cost. Also, the current experimental design is still in its early stages of development and some changes maybe be necessary to improve the mold. The wooden pieces of the molds were wrapped in polyethylene sheets

to avoid water absorption from the cement paste during the experiment. Current mold design worked well with all of the different types of reinforcements presented herein.

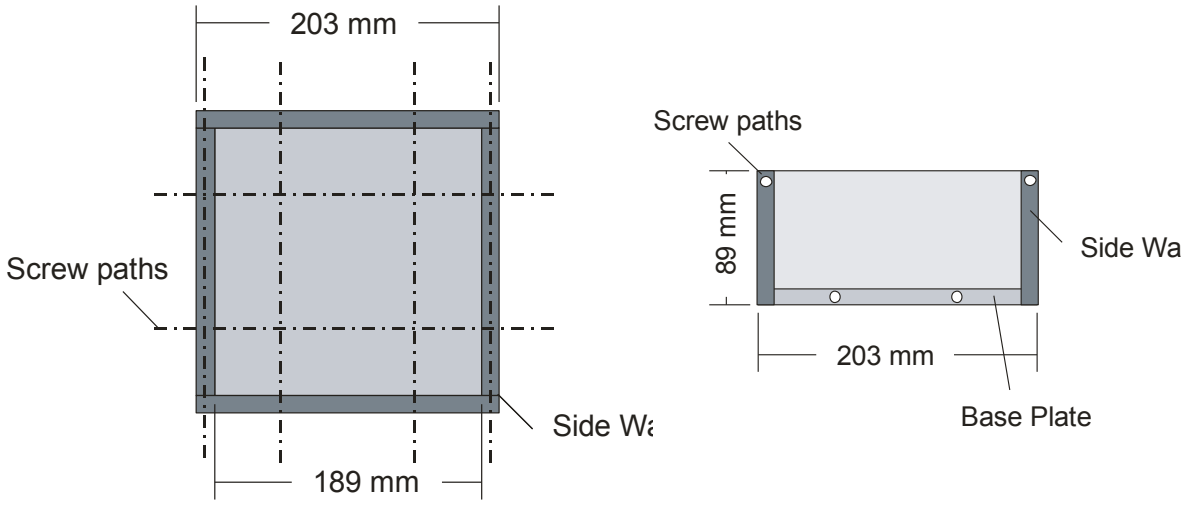

(a) (b)

Figure 4.2 – Geometric Configuration of the New Mold: a) plan view, b) x-s view

4.2.3 Specimen Size

Two different specimens sizes were considered, namely: 178x178x89 mm (7”x7”x3”) and 178x178x25 mm (7”x7”x1”). The difference between the specimens is shown in Figure 4.3. The same mold was used for the two specimen sizes. The specimen size was determined during the mixing procedure, wherein the mixing material was filled up to the 89mm (3”) mark or the 25 mm (1”) mark of the mold. Initially 178x178x89 mm (7”x7”x3”) specimens were used so as to try to simulate typical slab-on-grade (SOG) or traditional concrete placement. Preliminary tests indicated that 89mm (3”) thick samples were too thick for most of reinforcement types. Only heavily reinforced specimens produced cracking patterns, but such types of cracks were expected and did not satisfy random cracking criteria. For most of the other types of reinforcement, evaporated water at the surface was constantly replaced by the water diffused through the

thickness of the specimen, which did not produce enough shrinkage to cause cracking. Due to these unsatisfactory results the depth of the specimen was reduced to 25 mm (1"). The subsequent smaller sized specimens produced more desirable results. It should be noted that the cracking patterns were affected by the type of reinforcement used. Therefore, some of the more effective reinforcement trials attained from the 178x178x25 mm (7”x7”x1”) were also tested for the 178x178x89 mm (7”x7”x3”) specimens.

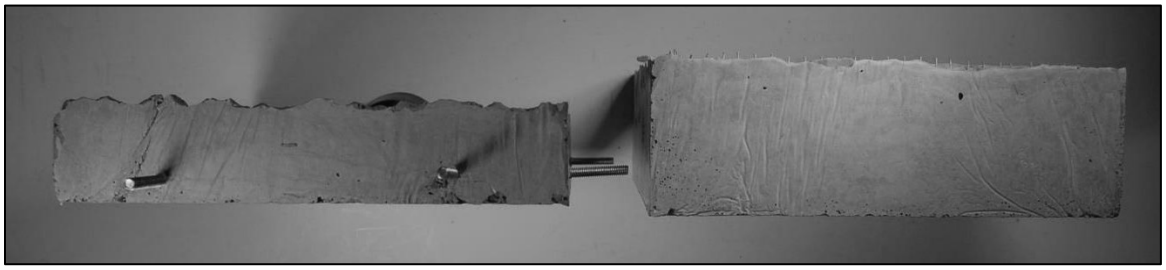

Figure 4.3 – Comparison between 178x178x25 mm and 178x178x89 mm Specimens

4.2.4 Manufacturing and Assembly of the Reinforcement

One of the most important factors that cannot be overlooked is the mold-reinforcement interactions. The need of the reinforcement to be removable emerged from the initial trials of the reinforcement design. In practice, the removal of the dried specimen out the mold can lead to the destruction of both the mold and the reinforcement. Therefore, the need to increase the life of the mold and make the reinforcement disposable led to several different possibilities: free, fixed, and semi-fixed fixity conditions. Free reinforcement consisted of a design that was freely inserted into and not connected to the mold; fixed reinforcement included a design that connected to the mold by means of bolts and nuts; semi-fixed reinforcement was connected to the mold by the means of hooks through or on the top of the mold.

Several different types of materials were used to prepare the reinforcements; these included crafting wood, zinc wire, hardware cloth and thin zinc plates. Figure 4.4 shows the material used, wherein size scale is shown for comparison. Preparation of the materials consisted of cutting the materials to specified length, depths and thicknesses. Some of the reinforcement styles were manufactured out of the same materials; others included some or all of the material types. Depending on the type of material and style of reinforcement, diverse manufacturing techniques were applied. This included weaving, wrapping, gluing and bending of the materials. In addition to the reinforcement material, cost and approximate time of construction and attachment of the reinforcement to the mold has been recorded and is reported later in this chapter.

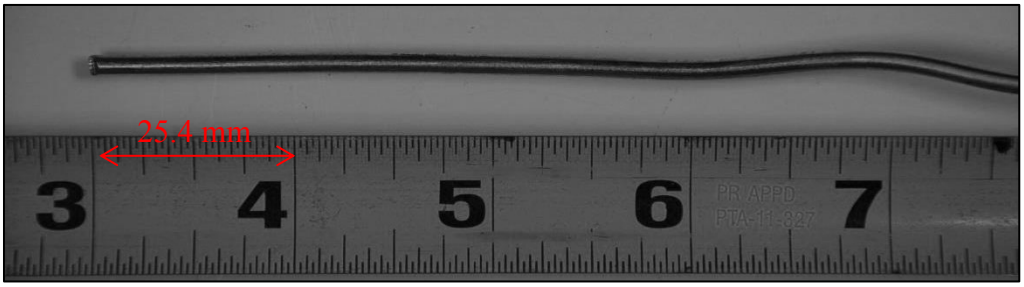

(a)

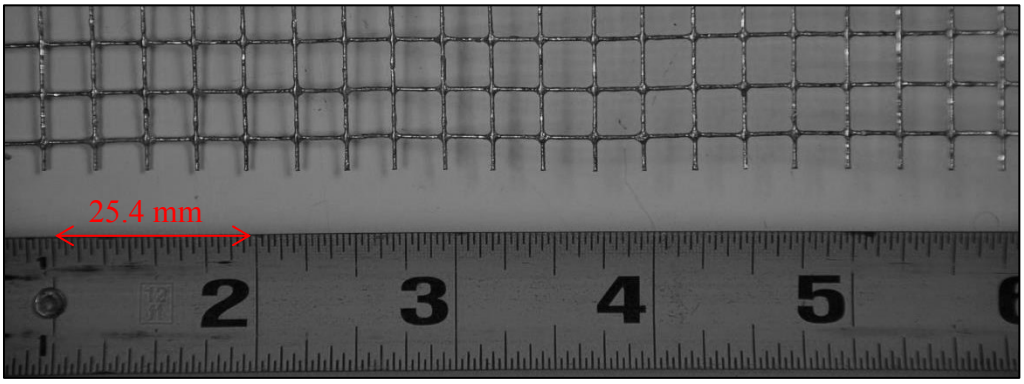

(b)

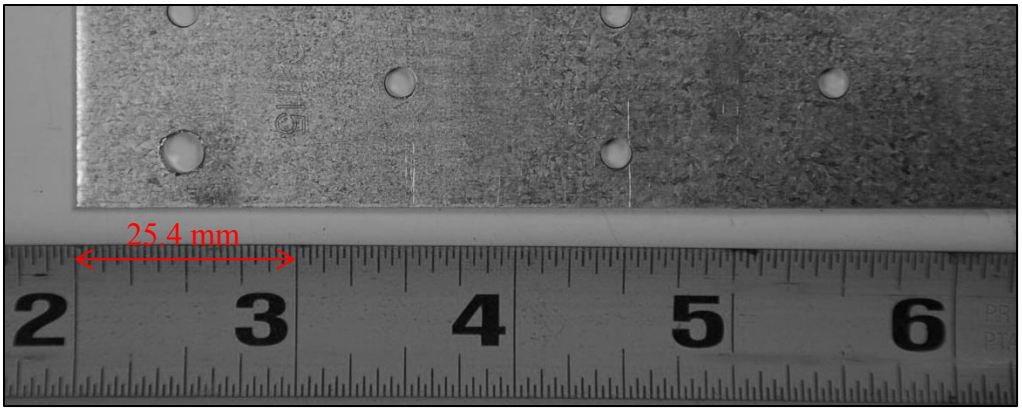

(c)

Figure 4.4 – Materials Used for Reinforcement Purposes: a) wire, b) hardware cloth, c) plates

4.3 Reinforcement Styles

4.3.1 Free

Free type of reinforcement consisted of strain localization independent of the reinforcement location. The reinforcement was simply inserted into the mold without any connection to the mold. In the absence of rigid connection between the mold and the reinforcement, cementitious paste outside the reinforcement zone would provide the stability and rigidity, while the paste inside the reinforcement experiences the imposed strain. Once the shrinkage was initiated, cement within the reinforcement zone would be restricted to the movement and start experiencing tensile stresses. Therefore, the cracking would occur within the reinforcement zone and provide random and potentially nonhomogeneous cracking. To satisfy two dimensional cracking criteria, the reinforcement was placed along the boundaries of the mold; additional reinforcement within the shrinkage zone was also designed with respect to the symmetry. Three different types of reinforcement were experimented with, wherein hardware cloth and the

zinc wire was used. Three reinforcements are shown in Figure 4.5 with proper labeling of the materials used. It should be noted plan view is presented for comparison purposes between the reinforcement. In all the three types of the reinforcement pre-cut piece of hardware cloth was bent to form a square; the pre-cut length of the cloth allowed to create perimeter that consisted of two layers of the cloth. The description of the reinforcement is as the following: Type 1 consisted only the perimeter reinforcement through the specimen thickness; Type 2 consisted of Type 1 reinforcement with additional crack zone surface reinforcement consisted of wire which was hooked onto the perimeter (referred to as heavy reinforcement); Type 3 consisted of Type 1 with single mid-section reinforcement through the specimen thickness, which consisted of the same hardware cloth as the perimeter.

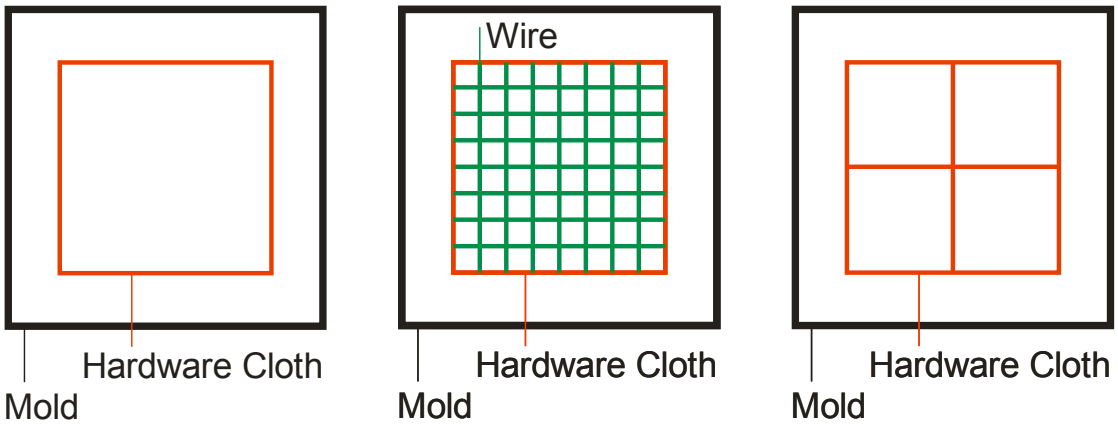

(a) (b) (c)

Figure 4.5 – Free Style Reinforcement Variation: a) Type 1, b) Type 2, c) Type 3

4.3.2 Fixed

Fixed type of reinforcement also consisted of strain localization but with respect to the rigid fixity of the reinforcement to the mold. The reinforcement was inserted into the mold and then connected to the mold using bolts and nuts through pre drilled holes in

the walls of the mold. In the presence of rigid connection between the mold and the reinforcement, the mold itself provided the stability and rigidity which was transferred into the reinforcement material; additional rigidity was expected in this configuration. Once the specimen cast inside the mold starts shrinking, the rigid mold-reinforcement mechanism would limit the movement of the specimen and thus also impose tensile stresses. These reinforcements were also designed in symmetrical fashion along the perimeter of the mold, that would provide random and nonhomogeneous cracking. Three different types of reinforcement were experimented with, wherein hardware cloth, zinc plates (with holes preinstalled), and wood plates were used. Three reinforcements are shown in Figure 4.6 with proper labeling of the materials used. Again, plan view is presented for comparison purposes between the different reinforcement schemes. Same technique was used to create the perimeter as described in the previous section. The description of the reinforcement is as the following: Type 1 consisted of only perimeter reinforcement through the specimen thickness of hardware cloth or plates connected to the mold; Type 2 consisted of Type 1 reinforcement albeit much closer to the boundaries of the mold, and Type 3 consisted of Type 1 design, but wood plates was used as the reinforcing material though the mid-section; wood plates were installed up to 2/3 of the total through the specimen thickness to work as stress risers. It should be noted that Type 3 which is similar to ASTM C1579 was designed with an idea of stress concentration rather than stress localization.

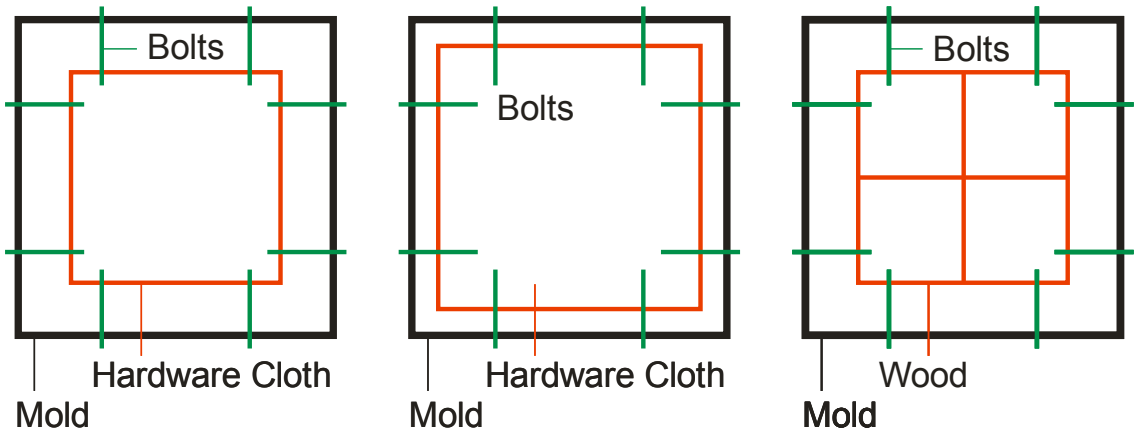

(a) (b) (c)

Figure 4.6 – Fixed Style Reinforcement Variation: a) Type 1, b) Type 2, c) Type 3

4.3.3 Semi-Fixed

Semi-fixed type of reinforcement also consisted of strain localization but involves rigid fixity between reinforcement-mold and the ease in installation/removal of the reinforcement. The reinforcement was inserted into the mold through pre-drilled holes in the sides of the mold or by means of hooking the reinforcement onto the walls of the mold. After the desired positioning, the reinforcement was bent to restrict its movement and provide necessary rigidity along the boundary. Similar to the free and fixed reinforcement styles, semi-fixed reinforcement would limit the movement of the cement, resulting in tensile stresses, which ultimately promotes formation of distributed two-dimensional cracks. These reinforcements were also designed in symmetrical fashion that would provide random and nonhomogeneous cracking. Three different types of reinforcement were experimented with, wherein only zinc wire was used. Three reinforcement styles are presented in Figure 4.7. The description of the reinforcement is as the following: Type 1 consisted of symmetrically spaced grid near the surface of the specimen connected to the top of the mold through hooks. Type 2 consisted of

symmetrically spaced individual brackets, two per each wall of the mold, which were connected through the wall of the mold. Type 3 consisted of single bracket per each side of the mold connected through the wall of the mold, spaced mid-way through the specimen thickness.

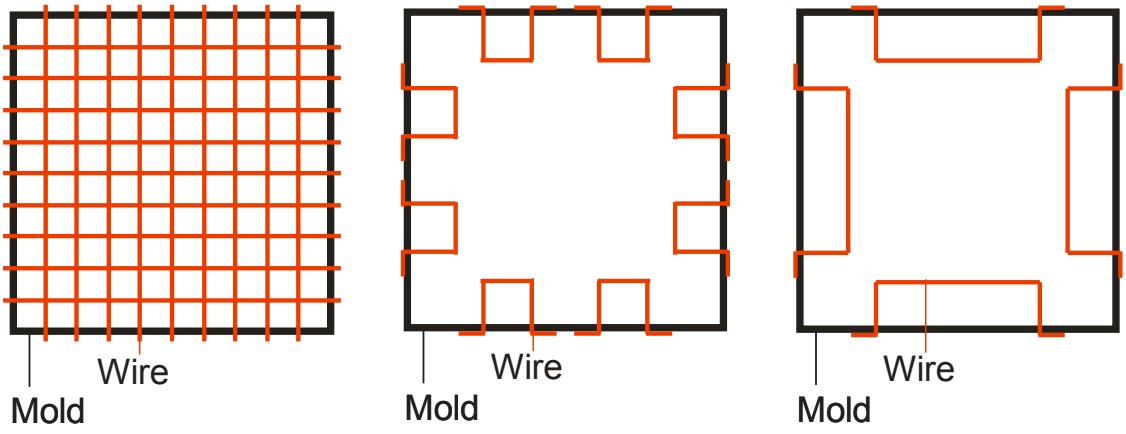

(a) (b) (c)

Figure 4.7 – Semi-Fixed Reinforcement Variation: a) Type 1, b) Type 2, c) Type 3

4.4 Preliminary Testing Results

The summary of the preliminary testing is shown in Table 4.1, wherein all of the variations of the reinforcements are presented with respect to construction time and success of the experiment. Only paste formulation was used for the preliminary tests as that allows formation of extensive shrinkage cracks. Table 4.1 indicates that most of the reinforcements tested on the 178x178x89 mm size specimens did not produce any cracking. As discussed before, heavily reinforced sections were the only ones that yielded any cracking in the 178x178x89 mm specimens, but the cracking patterns produced were localized near the reinforcements. Therefore, such reinforcements were not considered for further study.

Table 4.1 – Preliminary Reinforcement Tests Results Summary

Mold	**Type**																	
	Free						**Fixed**						**Semi-fixed**					
Variation	**Type 1**		**Type 2**		**Type 3**		**Type 1**		**Type 2**		**Type 3**		**Type 1**		**Type 2**		**Type 3**	
Construction Time (hours)	0.5		1.25		1.0		0.75		0.75		2.0		1.5		0.75		0.25	
Specimen Thickness (mm)	25	89	25	89	25	89	25	89	25	89	25	89	25	89	25	89	25	89
Success (Y/N)	N	N	-	Y	-	Y	N	N	N	N	Y	Y	-	Y	Y	Y	Y	-

Figure 4.8 shows different types of reinforcement that did not produce any cracking. The short comings of the reinforcement presented in Figure 4.8 include not providing enough stiffness to restrict the shrinkage or not promoting the shrinkage to a level wherein desired cracking can occur. Figure 4.9(a) and Figure 4.9(b) shows the heavily reinforced cracking patterns on semi-fixed Type 1 and free Type 2 specimens, respectively. Additionally, fixed Type 3 reinforcement was also neglected for further study due to its cracking mechanism. Stress concentration was imposed on the specimen that caused predictable cracking pattern, which was not desirable for the simulation purposes. Figure4.9(c) shows the results of Fixed Type 3 reinforcement.

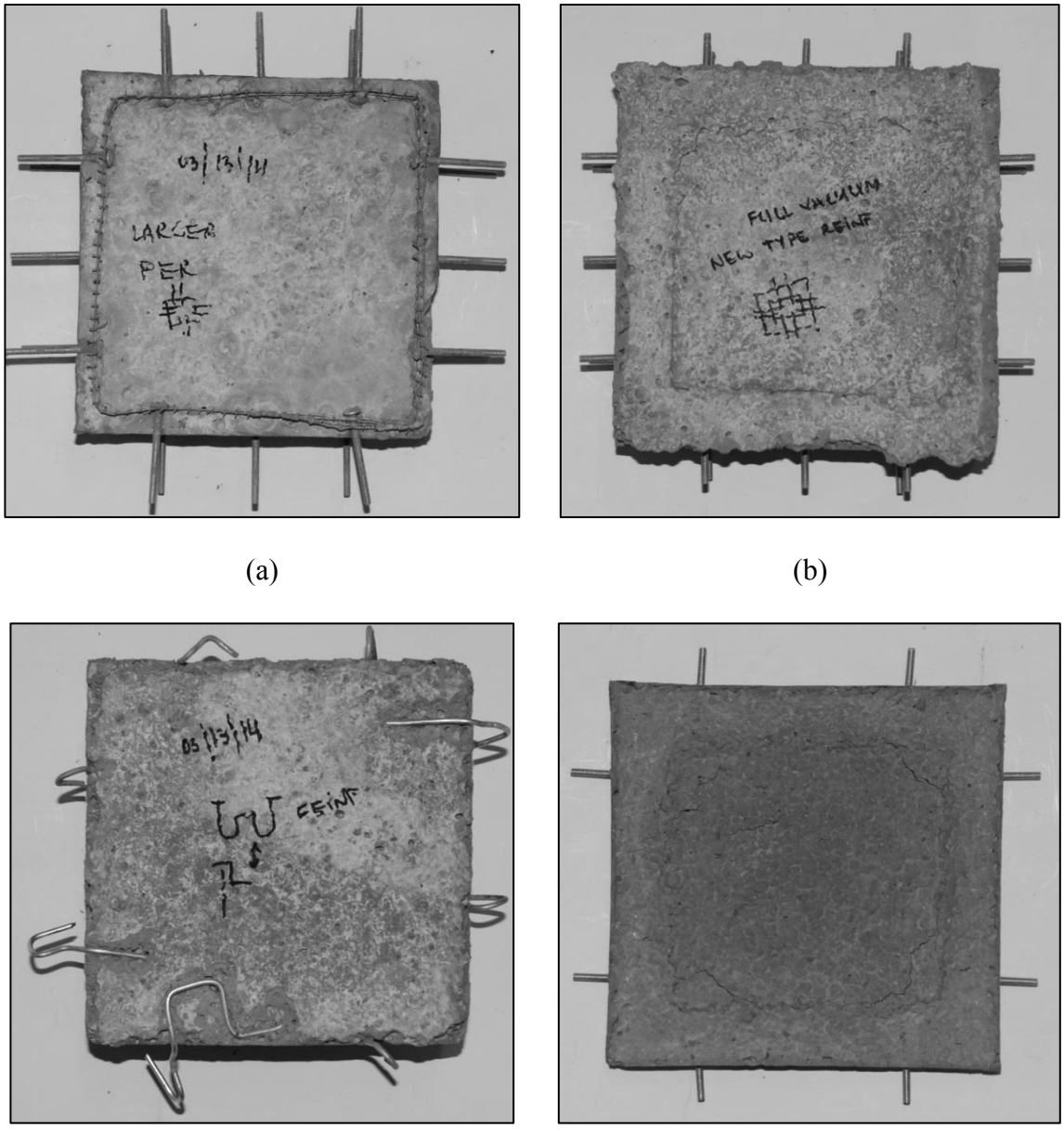

(a) (b)

(c) (d)

Figure 4.8 – Types of Reinforcements without Any Cracking: a) fixed Type 2 (mesh, 89mm thick), b) fixed Type 1 (plates, 89 mm thick), c) semi-fixed Type 2 (89 mm thick), d) fixed Type 2 (mesh, 25 mm thick)

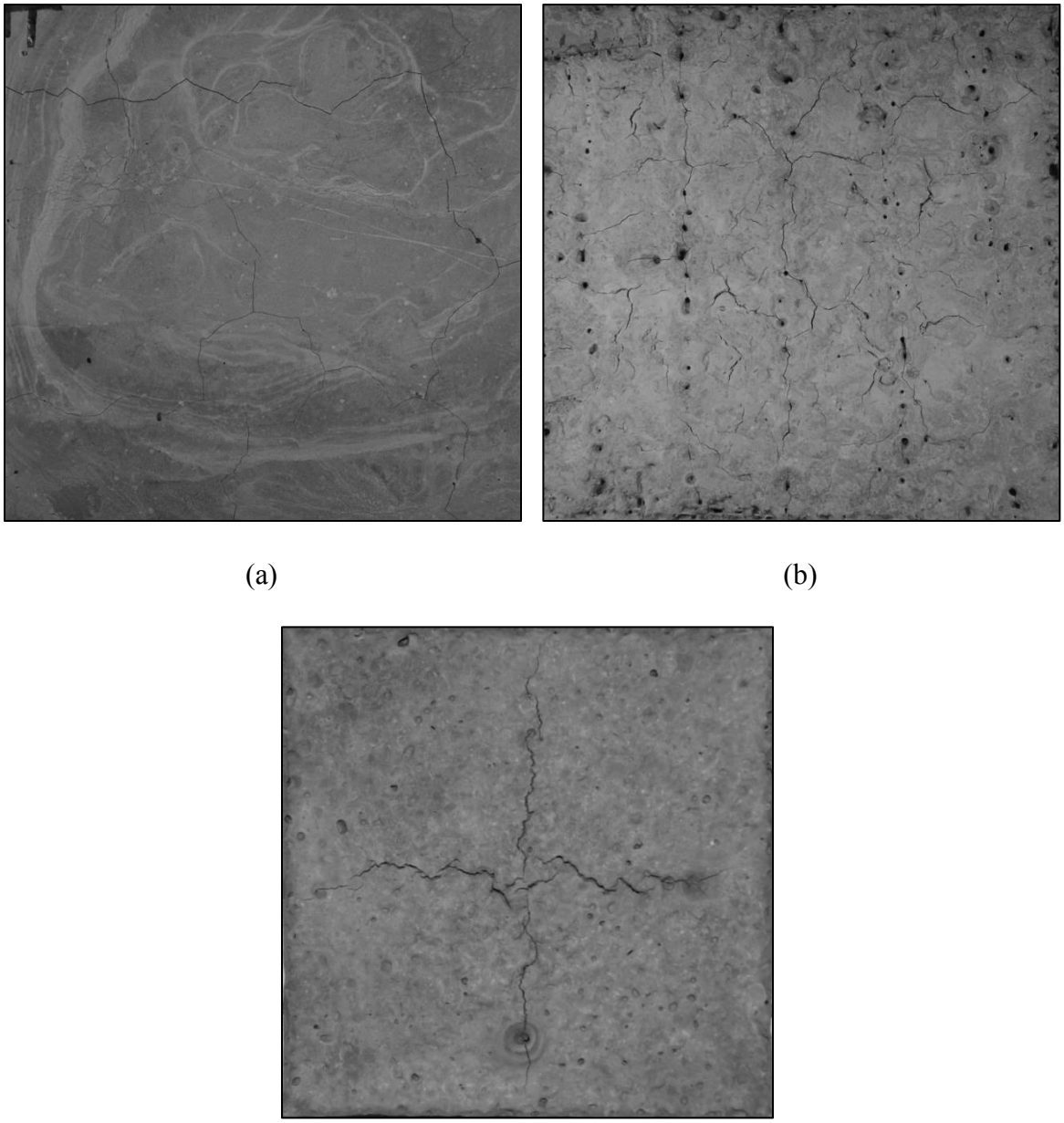

(a) (b)

(c)

Figure 4.9 – Undesired Cracking Pattern Produced from Preliminary Testing: a) semi-fixed Type 1 (89 mm thick), b) free Type 2 (89mm thick), c) fixed Type 3 (25 mm thick)

The leftover alternatives were now evaluated based upon construction time and the material use. Clearly, semi-fixed Type 3 reinforcement emerged as the best option. Due to its requirement of only one material, the zinc wire, shortest construction time and

the best results thus far, semi-fixed Type 3 reinforcement was shortlisted as the main reinforcement and was used for the testing of replicate specimens. Figure 4.10 presents a photograph of the reinforcement scheme. The reason why this type of reinforcement was successful is primarily due to the combinations of all of the ideas that emerged from the previous reinforcements by essentially trial and error method. Figure 4.11 shows the results obtained from semi-fixed Type 3 reinforcement, wherein the top and the bottom surfaces of the specimens are shown. It should be noted that the cracks reached to the bottom of the 25 mm specimens.

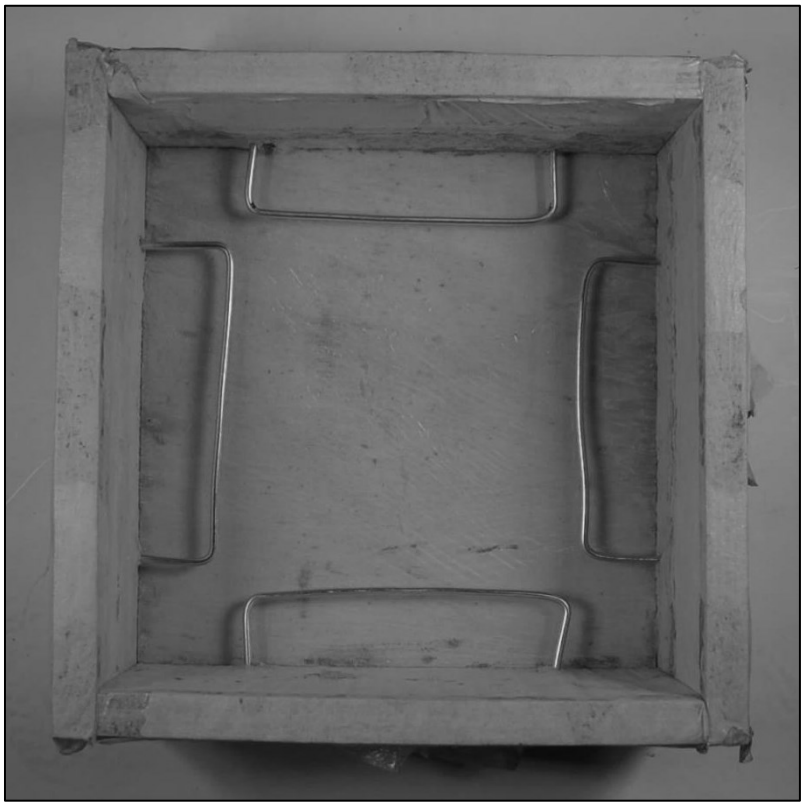

Figure 4.10 – Reinforcement Used for Replicates Testing

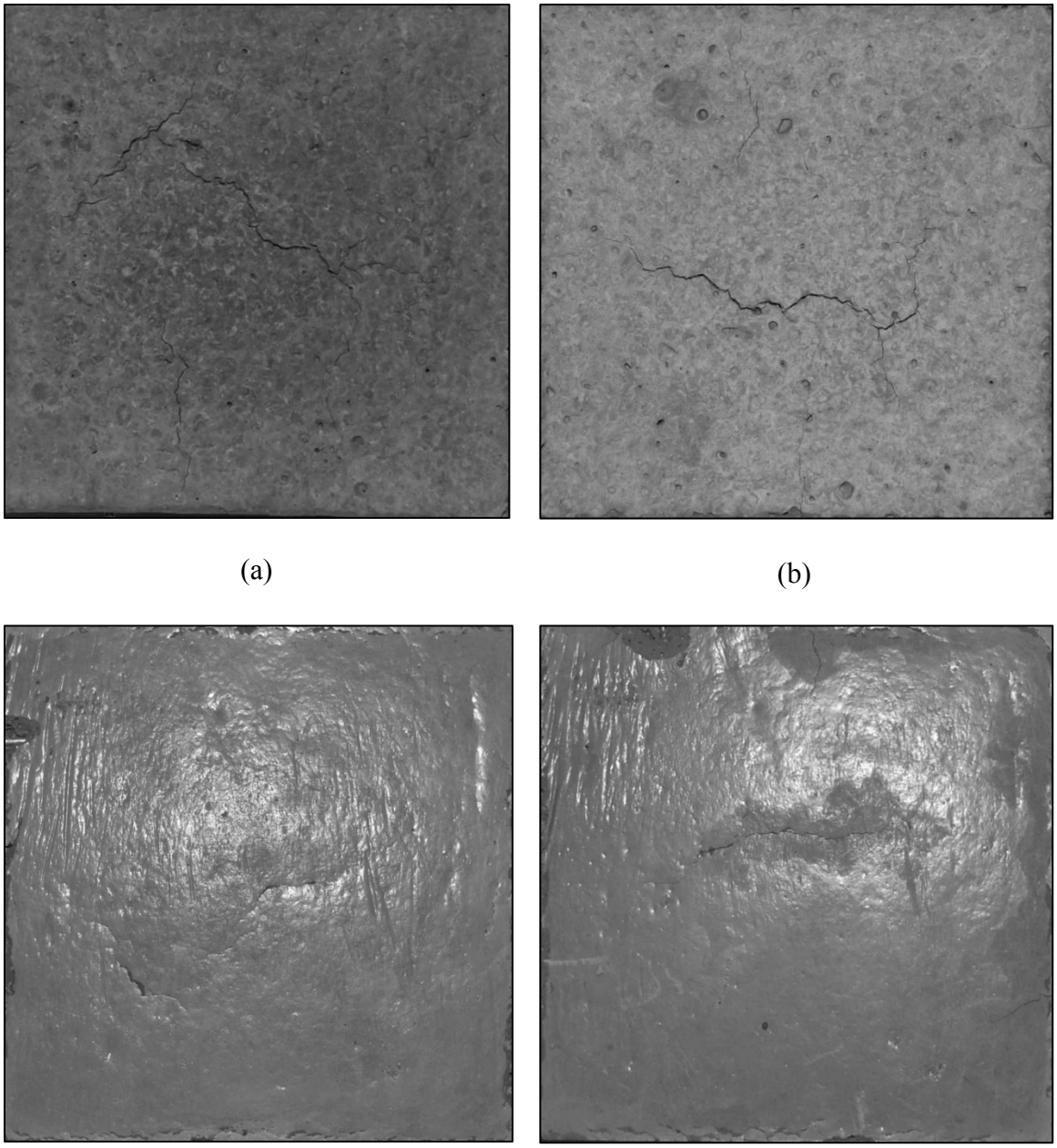

(a) (b)

(c) (d)

Figure 4.11 – Cracking Pattern Produced by Semi-Fixed Type 3 Reinforcement: a) replicate 1 top surface, b) replicate 2 top surface, c) replicate 1 bottom surface, d) replicate 2 bottom surface

4.5 Experimental Program

The experimental program thus far consisted of evaluating paste and mortar specimens of 178x178x25 mm size. Paste specimens consisted of Portalnd cement (Type II/V) and water with a w/c ratio of 0.45; mortar specimens consisted of Portalnd cement, fine silica sand and water with c/s ratio of 1 and w/c ratio of 0.5. The details of mix proportioning are provided in Table 4.2. It should be noted that w/c ratio was attempted to stay constant, but due to the presence of sand within the mortar mix, water content was slightly adjusted to produce similar workability as the paste specimens. The mixing procedure consisted of mixing the dry ingredients, followed by the addition of water and additional mixing at higher speed, until desired consistency was achieved. Fresh cementitious paste was then immediately poured in the molds for the vacuum evaporation test.

Table 4.2 - Mix Design for Larger Shrinkage Tests

Constituents	Percentage (%)		Proportions by 1000 g of Cement	
	Paste	Mortar	Paste	Mortar
Portland Cement	31	40	1000	1000
Silica Sand	0	40	0	1000
Water	69	20	450	500

4.6 Results and Discussion

4.6.2 Evaporation

Three replicates were made for paste specimens and one replicate was made for the mortar specimen. For discussion purposes only representative specimen from paste replicates is presented. Figure 4.12(a) shows the cumulative moisture loss and Figure

4.12(b) shows the evaporation rates of the two samples. Due to the size of the specimen, the test was conducted for 72 hours in order to obtain moisture loss curves that are similar to the smaller size specimens, which were tested for only 24 hours. It is evident from Figure 4.12 that the response of the three different specimens is similar, however, quantified values of moisture loss and evaporation rates are very different. Larger specimens produced much higher cumulative moisture loss which can be justified with increased thickness of the specimen. Evaporation rate is much lower than that of a smaller specimen. Initial evaporation rate is decreased by a factor of 2 for larger size specimens. Such phenomena can be justified by the increase in the surface area of the specimen. The more interesting trend can be observed when large paste and mortar specimens are compared. A decrease of 20 % and 18 % was observed in cumulative moisture loss and evaporation rate. Additionally, the evaporation rate reduces in the presence of sand when the large specimens are compared.

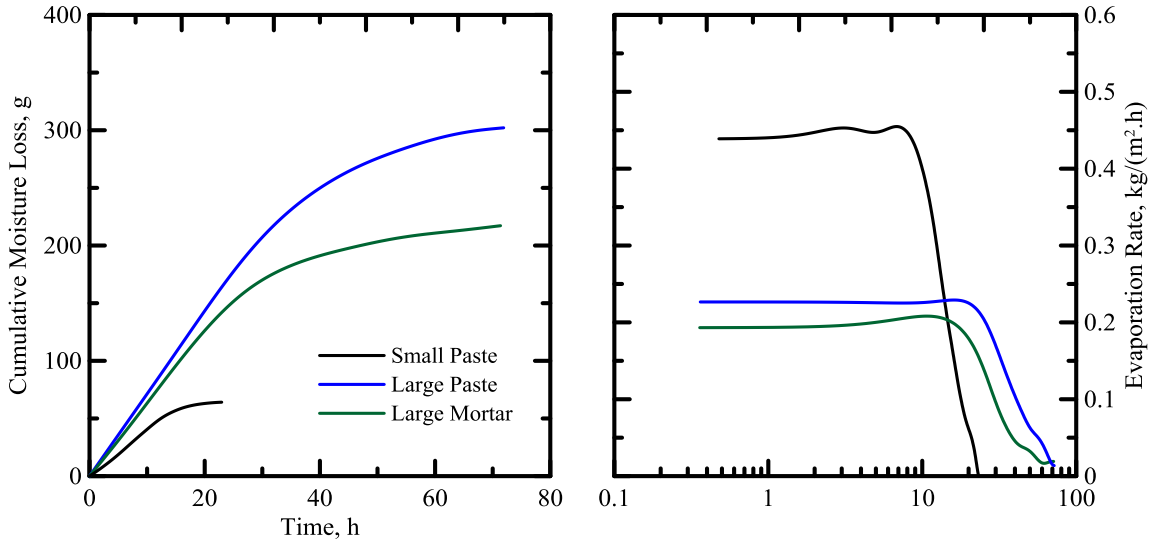

Figure 4.12 - Effect of Specimen Size and Composition on Evaporation Tests Results: a) cumulative moisture loss, b) evaporation rate

Large and small sized specimens can be also compared on the basis of normalized cumulative moisture w.r.t total amount of cement paste used. This relationship is shown in Figure 4.13. Figure 4.13 indicates a different trend, wherein smaller specimens have more moisture loss per gram of cement paste used when compared the large size specimens; about 12 % when paste specimens are compared. This can be explained in the context of higher evaporation rate and smaller surface area. It is also observed that mortar specimens exhibit 8 % increase in normalized cumulative moisture loss which may suggest increase in the extent of shrinkage cracks. However, as shown in the next section, due to the presence of the sand within mortar specimens, the extent of shrinkage cracking is reduced.

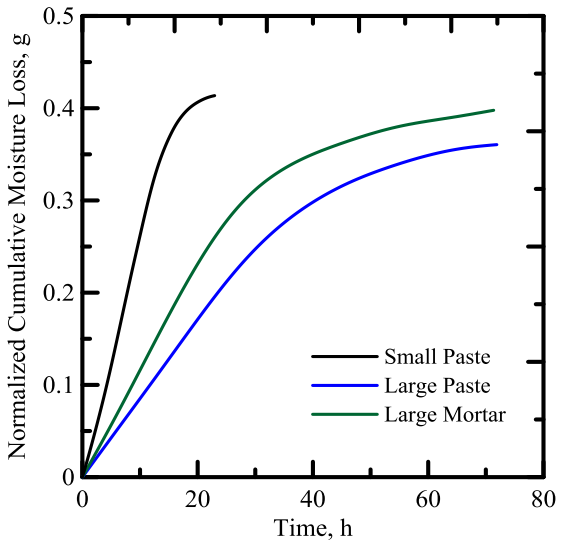

Figure 4.13 - Effect of Specimen Size and Composition on Normalized Cumulative Moisture Loss

4.6.3 Crack Morphology

Similarly to drying properties, crack morphology was evaluated for the larger size specimens. Representative cleaned-up binary images are presented for paste and mortar

specimens respectively in Figure 4.14. The crack morphological results are summarized in Table 4.3. It is observed that all of the shrinkage crack morphology parameters are lower for the mortar specimens. This can be justified by the presence of the sand in the mix. Since the amount of paste available for shrinkage within mortar specimens is less than that of the paste specimens, less cracking occurs.

Table 4.3 - Crack Morphology Parameters Summary of Large Shrinkage Specimens

Crack Properties	Small	Large	
	Control	**Paste**	**Mortar**
Length of cracks (mm)	955 ± 45	667 ± 70	595
Area of cracks (mm^2)	303 ± 35	267 ± 15	184
Density of cracks (mm^{-1})	0.096 ± 0.004	0.021 ± 0.002	0.019
Mean crack length (mm)	0.608 ± 0.034	0.838 ± 0.243	0.382
Crack are fraction (-)	0.030 ± 0.004	0.008 ± 0	0.006
Width of cracks (mm)	0.318 ± 0.051	0.404± 0.033	0.309

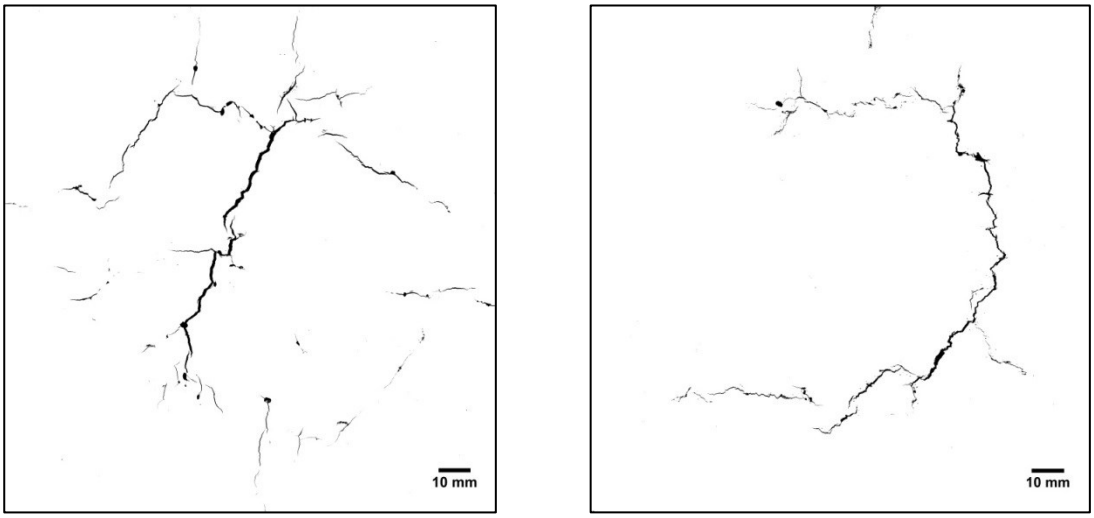

(a) (b)

Figure 4.14 - Cleaned Up Binary Images of Representative Large Specimens: a) paste, b) mortar

The more interesting results arise when larger shrinkage specimens are compared to smaller shrinkage specimens. The typical crack parameters presented in previous chapter are a good basis for comparison of the same size specimen. However, to compare two different size specimens, parameters such as crack density and crack area fraction are needed (crack density is defined as the ratio of length of the crack with respect to the total area of the image and crack area fraction is defined as the ratio of crack area with respect to the total area of the image). The comparison between paste small, paste large and mortar large specimens is shown in Figure 4.15, wherein crack density and crack area fraction are presented. It is evident that large size shrinkage specimens do not produce nearly the quantity of cracks that smaller size specimens do; the amount of crack is reduced by almost a factor of 4 per unit area. This result suggests that either the stresses induced from the shrinkage are not high enough to create as much cracking or the rate of evaporation per area of the specimen is not sufficient to provide the shrinkage needed.

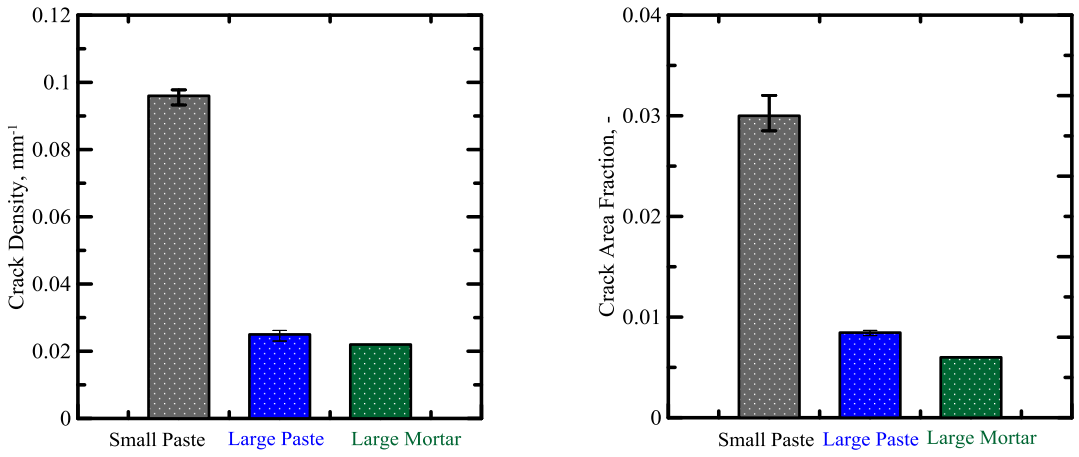

(a) (b)

Figure 4.15 - Effect of Specimen Size in Altering Early Age Shrinkage in Cement Based Specimens

4.7 Conclusion

Different reinforcement combinations on two different samples thicknesses were tested to determine restraining system to simulate drying and crack morphology properties of cement based composites. The data collected thus far provides results that suggest cumulative moisture loss is a function of the paste content. Similarly, assuming reinforcement mechanism worked the same way for both of the specimens, surface cracking is also a function of paste content. Mixing sand with cement paste decreases cumulative moisture loss for the composite nature of the mix, assuming nearly the same w/c ratio. Additionally, formation of cracks is also limited due to the presence of the sand that does not participate in the shrinkage process. In comparison with the smaller specimens, it is much harder to produce the same type of crack pattern on larger specimens. This outcome could be due to the reinforcement mechanism not providing enough restrain to produce higher stresses or the vacuum pumping equipment/hoses for not producing enough pressure to evaporate and transport moisture from the larger surface area specimens. Further experimentation with other types of reinforcements, vacuum equipment and specimen variations is required to advance the simulation and acquire better, more accurate results that would reflect natural mechanism of cement based composites. This work could also be extended to concrete mixes with coarse aggregates, as that will enable us to predict the extent of shrinkage crack in real world applications.

5.0 REFERENCES

1. Horvath A. Construction materials and the environment. Annu RevEnviron Resour 2004; 29: 181-204.

2. Brameshuber W, Textile Reinforced Concrete, State-of-the-Art Report of RILEM Technical Committee 201-TRC, RILEM Report 36 2006; 1-271.

3. CEMBUREAU (the European Cement Association), Rue d'Arlon 55, BE-1040 Brussels, Belgium.

4. Kwon SJ, Na UJ, Park SS, Jung SH. Service life prediction of concrete wharves with early-aged crack: Probabilistic approach for chloride diffusion. Struct Saf 2009; 31(1):75-83.

5. Huang XM, Yang CY. Early-age concrete cover crack and its effects on concrete cover. Key Eng Mater 2006; 302-303:630-6.

6. Yoon IS, Schlangen E, de Rooij MR, van Breugel K. The effect of cracks on chloride penetration into concrete. Key Eng Mater 2007; 348-349:769-72.

7. Lura P, Pease B, Mazzotta GB, Rajabipour F, Weiss J. Influence of shrinkage-reducing admixtures on development of plastic shrinkage cracks. ACI Mater J 2007; 104(2):187-94.

8. Banthia N, Gupta R. Plastic shrinkage cracking in cementitious repairs and overlays. Mater Struct 2009; 42(5):567-79.

9. Mora-Ruacho J, Gettu R, Aguado A. Influence of shrinkage-reducing admixtures on the reduction of plastic shrinkage cracking in concrete. Cem Concr Res 2009; 39(3):141-6.

10. Cohen MD, Olek J, Dolch WL. Mechanism of plastic cracking in portland cement and portland cement-silica fume paste and mortar. Cem Concr Res 1990; 20(1):103-19.

11. Mehta PK, Monteiro PJM. Concrete: Microstructure, Properties and Materials. Boston: McGraw-Hill, 2006.

12. Slowik V, Schmidt M, Fritzsch R. Capillary pressure in fresh cement based materials and identification of the air entry value. Cem ConcrCompos 2008; 30:557–565.

13. Radocea A. A study on the mechanism of plastic shrinkage of cement based materials. PhD thesis, Göteborg, Chalmers University of Technology, Göteborg; 1992.

14. Wittmann FH. On the action of capillary pressure in fresh concrete, Cem Concr Res 19766; 6(1):49–56.

15. Esping O. Effect of limestone filler BET(H2O)-area on the fresh and hardened properties of self-compacting concrete, Cem Concr Res 2008; 38:938–944.

16. Morris P, Dux P. Cracking of plastic concrete, Aust J Civ Eng 2003; 1(1):17-21.

17. Aly T, Sanjayan JG. Mechanism of early age shrinkage of concretes, Mater Struct 2009;42:461–468.

18. Hammer TA. Effect of silica fume on the plastic shrinkage and pore waterpressure of high-strength concretes, Mater Struct 2001; 34:273-278.

19. Wongtanakitcharoen T, Naaman AE. Unrestrained early age shrinkage of concrete with polypropylene, PVA, and carbon fibers, Mater Struct2007; 40:289-300.

20. Benboudjema F. Modélisation des déformations différées du béton sous solicitations biaxiales. Application aux enceintes de confinement de bâtiments réacteurs des centrales nucléaires, PhD dissertation, Université de Marne-la-Vallée, 2002.

21. Grzybowski M, Shah S. Shrinkage Cracking of Fiber Reinforced Concrete. ACI 1990; 81(2):138-148.

22. Qi C, Weiss J, Olek J. Characterization of plastic shrinkage cracking in fiber reinforced concrete using image analysis and a modified Weibull function. Materials and Structures 2003; 36(260):386-395

23. Banthia N, Azzabi M, Pigeon M, Restrained shrinkage cracking in fiber reinforced cementitious composites, Materials and Structures Rilem 1993; 26(161): 405-413.

24. Soroushian P, Ravanbakhsh S. Control of plastic shrinkage cracking with specialty cellulose fibers, ACI Mater J 1998; 95(4):429-35.

25. Naaman A, Wongtanakitcharoen T, Hauser G. Influence of different fibers on plastic cracking of concrete. ACI 2005; 102:49-58.

26. Banthia N, Yan C. Shrinkage crackingin polyolefin fiber-reinforced concrete. ACI 2000; 97:432-437.

27. Sanjuan MA, Moragues A. A testing method for measuring plastic shrinkage in polypropylene fibre reinforced mortars. Mater Lett 1994; 21:239-46.

28. Nanni A, Ludwig DA, Mcgillis MT. Plastic shrinkage cracking of restrained fiber-reinforced concrete. Transp Res Rec 1993; 1382:69-72.

29. Naaman AE, Wongtanakitcharoen T, Hauser G. Influence of different fibers on plastic shrinkage cracking of concrete. ACI Mater J 2005; 102(1):49-58.

30. Ma Y, Zhu B, Tan M, Wu K. Effect of Y type polypropylene fiber on plastic shrinkage cracking of cement mortar. Mater Struct 2004; 37:92-5.

31. Jacobsen S, Aarseth LI. Effect of wind on drying from wet porous building materials surfaces-A simple model in steady state. Mater Struct 1999; 32:38-44.

32. Shimomura T, Maekawa K. Analysis of the drying shrinkage behavior of concrete using a micromechanical model based on micropore structure of concrete. Mag Concr Res 1997; 49(181):303-322.

33. Bakhshi M , Mobasher B. Experimental observations of vacuum drying of early-age Portland cement paste. Cement and Concrete Composites 2011; 31:474-484.

34. Bakhshi M, Mobasher B, Soranakom C. Moisture Loss Characteristics of Cement-Based Materials under Early-Age Drying and Shrinkage Conditions. Construction and Building Materials 2012; 30:413–425.

35. Ransinchung GD, Kumar B, Kumar V. Assessment of water absorption and chloride ion penetration of pavement quality concrete admixed with wollastonite and microsilica. Construction and Building Materials 2009; 23:1168 – 1177.

36. NYCO Minerals, Physical properties of Wollastonite,[Online], Available: http://www.nycominerals.com/files/Physical-Properties-Overview.pdf

37. Beaudoin JJ, Low N. Flexural strength and microstructure of cement binders reinforced with wollastonite micro-fibres. Cement and Concrete Research 1993; 23, 905-916.

38. Beaudoin JJ, Low N. The flexural toughness and ductility of portland cement-based Binders reinforced with wollastonite micro-fibres. Cement and Concrete Research 1194; 24(2):250-258.

39. NYO Minerals, Chemical and physical properties of Wollastonite,[Online],Available:http://www.nycominerals.com/wollastonite-chemical-composition-chemical-physical-properties

40. Copeland LE, Hayes JC. Determination of non-evaporable water in hardened Portland-cement paste. *ASTM Bulletin* 1953; 194:70-4.

41. Crank J. The mathematics of diffusion. New York: Oxford Science Publications, 1989.

42. Mathwork file exchange, Matlab Central (2003), Skeleton Intersection Detection, [Online], Available: http://www.mathworks.com/matlabcentral/fileexchange/4252-skeleton-intersection-detection

43. Beaudoin J J, Low N. Mechanical properties of high performance cement binders reinforced with wollastonite micro-fibres. Cement and Concrete Research 1992; 22: 981-989.

44. Dey V, Kachala R.,Bonakdar,A.,Mobasher,B. Wollastonite Nano-Fiber in Cementitious Composites, manuscript in preparation.

45. Cook R, Hover K. Mercury porosimetry of hardened cement pastes. Cem Concr Res 1999;29(6): 933-943.

46. Abell A, Willis K, Lange D. Mercury intrusion porosimetry and image analysis of cement-based materisl. J Colloid Interface Sci 1999; 211(1):39-44.

47. Garboczi E. Permeability, diffusivity, and microstructural parameters: A critical review. Cem Concr Res 1990; 20: 592-601.

48. Hegger J. Textile Reinforced Concrete. Proceedings of the 1st International RILEM Symposium. RILEM Proceedings PRO 50 2006; 1-389.

49. Häußler-Combe U, Jesse F, Curbach M. Textile Reinforced Composites – Overview, Experimental and Theoretical Investigations. Proc., 5th International Conference on Fracture Mechanics of Concrete and Concrete Structures, Ia-FraMCos 204; 749-756.

50. Mobasher B. Mechanics of Fiber and Textile Reinforced Cement Composites. CRC press 2011; 480.

51. Peled A, Mobasher B. Pultruded fabric-cement composites. ACI Materials Journal 2005; 102(1):15-23.

52. Mobasher B, Peled A, Pahilajani J. Distributed cracking and stiffness degradation in fabric-cement composites. Materials and Structures 2006; 39(287):317–331.